

Article

Spatiotemporal Dynamics of Forest Vegetation and Their Impacts on Soil Properties in the Forest-Steppe Zone of Central Russian Upland: A Remote Sensing, GIS Analysis, and Field Studies Approach

Yury G. Chendev ¹, Anthony R. Lupo ^{2,*}, Edgar A. Terekhin ¹, Maria A. Smirnova ³, Aleksandr N. Gennadiev ³, Anastasia G. Narozhnyaya ¹, Maria G. Lebedeva ¹ and Valery G. Belevantsev ¹

¹ Department of Nature Management and Land Cadaster, Institute of Earth Sciences, Belgorod State University, Pobeda Street 85, 308015 Belgorod, Russia; sciences@mail.ru (Y.G.C.); terekhin@bsu.edu.ru (E.A.T.); narozhnyaya_a@bsu.edu.ru (A.G.N.); lebedeva_m@bsu.edu.ru (M.G.L.); belaral@bk.ru (V.G.B.)

² Missouri Climate Center, Department of Soil, Environmental, and Atmospheric Sciences, University of Missouri, 302 Anheuser-Busch Natural Resources Building, Columbia, MO 65211, USA

³ Department of Landscape Geochemistry and Soil Geography, Faculty of Geography, Lomonosov Moscow State University, Leninskie Gory 1, 119330 Moscow, Russia; summerija@yandex.ru (M.A.S.); alexagenna@mail.ru (A.N.G.)

* Correspondence: lupoa0313@gmail.com

Abstract: This article showcases the outcomes of a comprehensive spatiotemporal dynamic analysis conducted in forest vegetation areas within the forest-steppe zone of the Central Russian Upland (eastern Europe), spanning the period from 1970 to 2020. This study utilized high-resolution data from the Corona satellite system from the year 1970 as well as satellite imagery from the ArcGIS World Imagery database. Soil properties and their changes were assessed based on the analysis of soil bulk density (930 samples), soil organic carbon features, pH, available phosphorus, and the composition of salt extracts (1362 samples). We collected and analyzed 3920 soil samples in the field to study the impact of shelterbelts on soil moisture over a period of two years. For six selected key sites with a total area of 1722 km², it was found that over a 50-year period, the area covered by forest vegetation increased from 14% to 24%. This expansion was primarily due to the planting and growth of young shelterbelts in the 1970s–1980s as well as widening anti-erosion shelterbelts on slopes and gullies. The average linear growth rate of forest vegetation boundaries was found to be 23.5 m (4.7 m per decade) for the entire study area. The expansion was highest on west-facing slopes, which was attributed to the higher moisture content from windward atmospheric precipitation events. However, alongside the increase in forest cover, degradation was also observed, particularly in old-age shelterbelts, which was attributed to increased fragmentation and mortality. A gradual increase in the extent of shelterbelt degradation was observed from the northwest to the southeast within the forest-steppe region, corresponding to areas with a drier climate. Additionally, the impact of shelterbelts on soil properties and soil cover was analyzed using four key sites and using fields and laboratory research methods. We detected a lateral uptake of substances from plowed soils into the soils of shelterbelts and vertical uptake from deep layers. The two-year observations (2020 and 2021) of soil moisture during the growing season (May–September) in two climatically contrasting forest-steppe areas revealed a more intensive accumulation of soil moisture in fields west of shelterbelts compared to those to the east of them, particularly within the 10 m zone near the shelterbelts. This can be attributed to arable fields on the windward side receiving more moisture compared to the leeward side. The formation of striped microstructures in the soil cover that occurred under the shelterbelts and on adjacent arable lands was influenced by various factors such as microclimatic conditions, vegetation types, ecological conditions for soil fauna, and human-induced soil processing and transformation along the shelterbelt boundaries. Shelterbelts and their adjacent areas in agro-landscapes are considered to be self-developing natural–anthropogenic geosystems with their own organizational structure. Therefore, their study is recommended as an integral part of modern geographical zoning.



Citation: Chendev, Y.G.; Lupo, A.R.; Terekhin, E.A.; Smirnova, M.A.; Gennadiev, A.N.; Narozhnyaya, A.G.; Lebedeva, M.G.; Belevantsev, V.G. Spatiotemporal Dynamics of Forest Vegetation and Their Impacts on Soil Properties in the Forest-Steppe Zone of Central Russian Upland: A Remote Sensing, GIS Analysis, and Field Studies Approach. *Forests* **2023**, *14*, 2079. <https://doi.org/10.3390/f14102079>

Academic Editor: Baozhang Chen

Received: 7 September 2023

Revised: 12 October 2023

Accepted: 13 October 2023

Published: 17 October 2023



Copyright: © 2023 by the authors. Licensee MDPI, Basel, Switzerland. This article is an open access article distributed under the terms and conditions of the Creative Commons Attribution (CC BY) license (<https://creativecommons.org/licenses/by/4.0/>).

Keywords: climate change; shelterbelts; agroforestry; afforestation; transformation of soils; Central Russian Upland

1. Introduction

Forests are the lungs of our planet and the main center of geochemical landscapes in the biosphere [1,2]. They are a focal point for geochemical processes on Earth due to the intense biological cycling of substances thanks to photosynthesis (the formation of organic matter) as well as the formation and decomposition of plant litter on the soil surface (the mineralization of dead organic residues) [3–6].

One of the most pressing environmental issues in the modern world is the reduction in forest areas due to human activities [7]. A striking example of forest reduction can be found in the forest-steppe zone of central eastern Europe [8]. According to a reconstruction based on various historical materials and maps from the pre-industrial period, the forest cover within the region was at least 40% of the total area (Figure 1). There were likely giant-sized oaks in broad-leaved forests with a diameter of three or more meters (Figure 2). This conclusion was based on the study of manuscripts from the 17th century, which indicated the sizes of boats made from whole tree trunks, with widths ranging from 1 to 3 “sazhens” and lengths from 5 to 10 “sazhens” (one “sazhen” equals 2.13 m) [9,10].

The forested area in the forest-steppe zone has been steadily declining over the centuries, as shown by a comparison of maps from the late 18th to the late 20th centuries (Figure 3). Measures to slow down forest degradation, study forest reproduction methods, and expand woody vegetation are important for the forest-steppe zone of eastern Europe, as well as many other regions worldwide [11,12].

Shelterbelts are critical components of agro-landscapes, functioning as natural–anthropogenic geosystems that influence various environmental factors. Understanding the spatiotemporal dynamics of shelterbelts and their impact on soil properties is essential for several reasons. Shelterbelts serve as effective anti-erosion measures, minimizing soil degradation and maintaining soil fertility, influencing the distribution of soil moisture, and performing nutrient cycling processes in soils, affecting nutrient availability for vegetation and agricultural crops [13–18] and others. They provide habitat and corridors for various plant and animal species, contributing to the conservation of biodiversity, and they form unique organizational structures within agro-landscapes [19,20]. Agroforestry has a clear advantage in combating global warming by effectively absorbing carbon from the atmosphere through the use of shelterbelts [21–23].

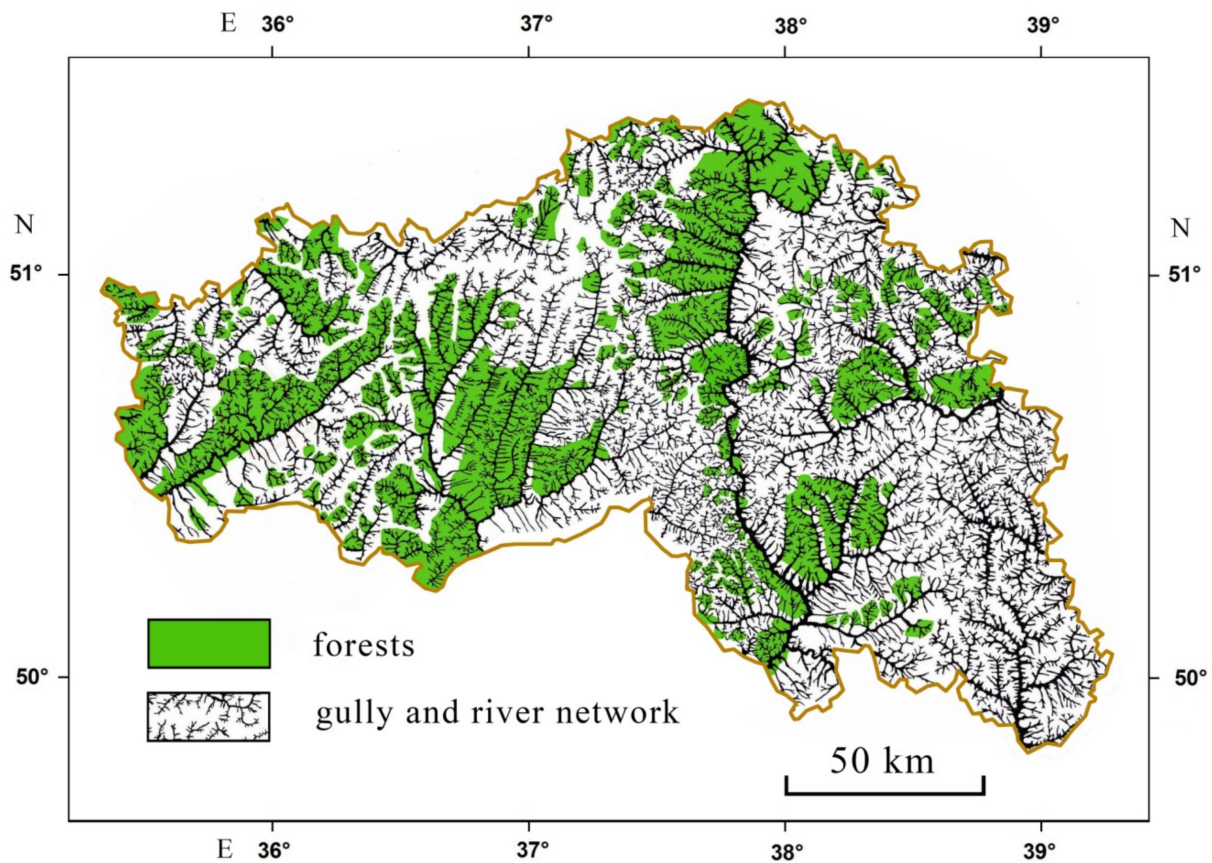


Figure 1. Forest cover prior to cultivation (17th century) of the center of eastern Europe (Belgorod region) (compiled by the authors based on various historical materials and maps).



Figure 2. Probable sizes of oaks that grew during the pre-agricultural stage in the forests of the Belgorod Oblast (reconstruction using computer graphics, authors' development).

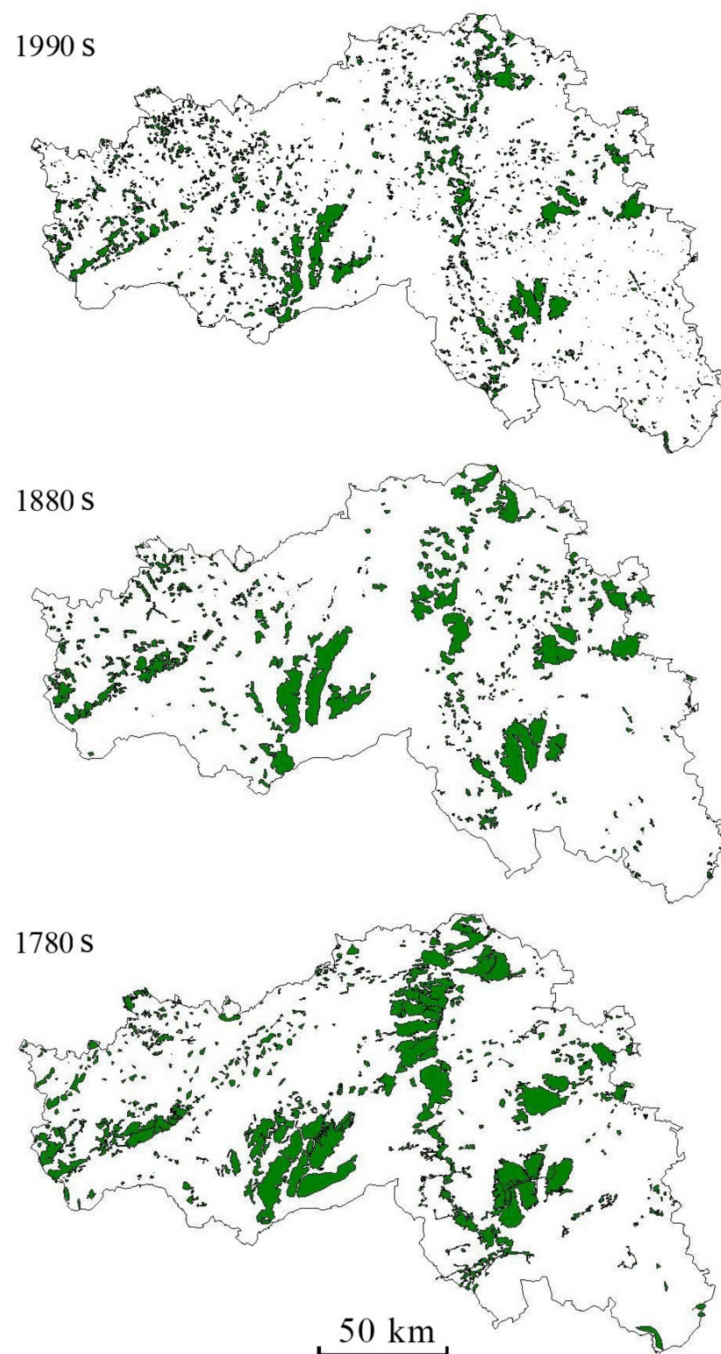


Figure 3. Forests of the Belgorod Oblast during different historical periods (compiled by the authors based on various temporal maps) (based on data from [24]).

Research on the diverse impact of shelterbelts within the environment has been conducted in the central forest-steppe zone of eastern Europe since the time of Vasily Dokuchaev, the founder of soil science. Dokuchaev's initiative in 1891 led to the establishment of the scientific experimental station "Kamennaya Steppe" in the southern part of the forest-steppe zone, which continues its research activities on a larger scale today [25–27]. Observations are conducted here for the components of the environment and ecosystems of shelterbelts planted at different times (Figure 4).



Figure 4. The (A) scientific town in Kamenaya Steppe (photo of a painting in the administrative building of the V.V. Dokuchaev Voronezh Federal Agrarian Scientific Center) and (B) a photograph of oak trees in one of the old-age shelterbelts in Kamenaya Steppe (photo by the authors).

The results of scientific research performed in the Kamennaya Steppe gained popularity in the United States after the infamous dust storms in the 1930s and during the implementation of the Soviet Union state plan for nature transformation [25,28]. The implementation of this grand plan covered the period from 1946 to the late 1980s. During this period, no less than 1.5 million hectares of shelterbelts for various purposes were planted across the territories of eastern Europe and Kazakhstan, including windbreaks and snow-retention belts on flat watersheds, anti-erosion plantations on slopes, protective plantings along highways and railways, and many others [18,29].

The shelterbelts created during the above-mentioned period continue to function to this day. The agricultural territory of the Belgorod region (total area—27.134 km²) can be cited as a worthy example of implementing the discussed state plan for the development of the shelterbelt system (Table 1).

Table 1. Changes in the area of shelterbelts within the boundaries of Belgorod Oblast during the period from 1955–2018, with units in hectares (ha).

Type of Shelterbelt	Year					
	1955 ¹	1965 ¹	1975 ²	1985 ²	2005 ³	2018 ⁴
Protective	29,500	34,490	18,190	20,990	23,200	23,200
Along ravines and gullies	4580	7110	61,700	67,210	67,100	67,300
Total	34,080	41,600	79,890	88,200	90,300	90,500

Note. Data from the archives: ¹ Committee for Land Affairs of the Belgorod Oblast; ² Land Surveying Service of the Belgorod Oblast; ³ Real Estate Management of the Belgorod Oblast; ⁴ Rosreestr Administration of the Belgorod Oblast.

However, interest in agroforestry as a government measure to support agriculture and protect soil from degradation has weakened in Russia since the 1990s [18]. As a result, several questions and problems have emerged that require attention. These include the

regeneration of aging and degraded shelterbelts, as well as the need to revive fundamental scientific research focused on gathering, analyzing, and organizing information regarding the changes in and patterns of soil properties influenced by shelterbelts.

Remote sensing data plays a crucial role in studying temporal changes in forested areas [30,31]. By obtaining satellite images of the Earth's surface, we are able to analyze forests over different time periods and gain insights into their spatiotemporal transformation [30,32,33]. GIS tools are employed to efficiently examine alterations in forest cover based on satellite imagery [24]. Furthermore, the integration of long-term satellite data with meteorological data allows us to explore the connections between climate characteristics and the dynamics of forest ecosystems. Through these approaches, we can acquire a comprehensive understanding of the changes occurring in forested lands over time [34,35].

The goal of our research is to analyze the contribution of shelterbelts to the contemporary afforestation within the central eastern Europe region as well as to study the transformation of soils in the shelterbelt influence zones.

2. Data and Study Region

Our study focuses on the (1) shelterbelts of agricultural landscapes in the southern part of the Central Russian Upland within the administrative boundaries of the Belgorod Oblast, Russia, and (2) the soils that are formed under the influence of these shelterbelts—both directly under the shelterbelts and at a short distance (up to 100 m) from them (Figure 5).

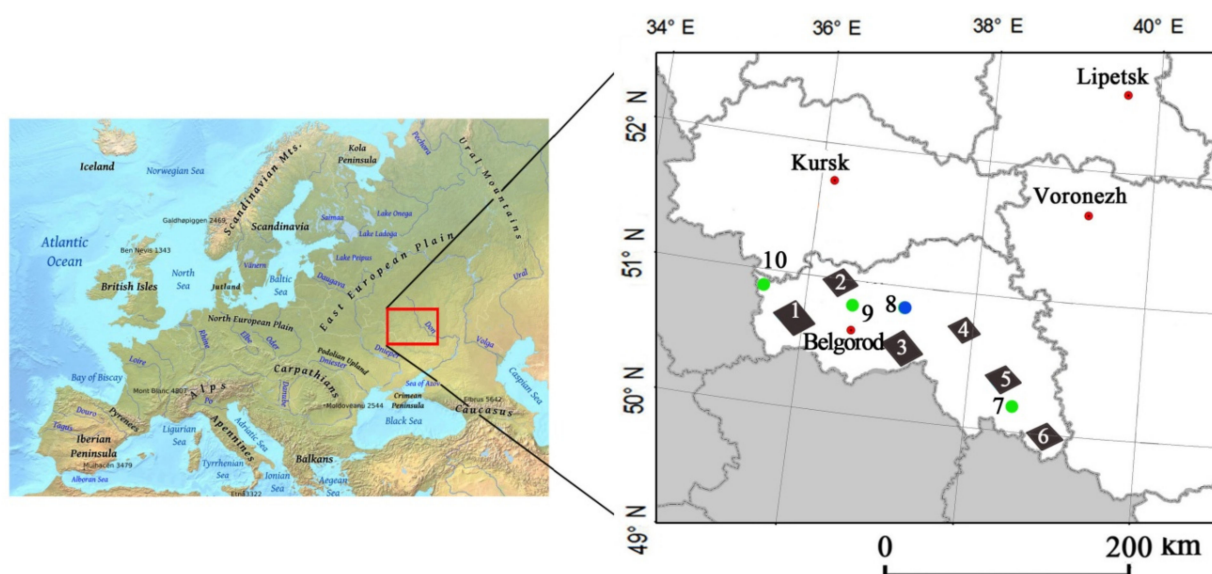


Figure 5. Scheme of key study sites: 1–6—areas for assessing the direction and rate of afforestation; 7–10—areas for studying the influence of shelterbelts on soil properties. 1—“Borisovsky”, 2—“Ivnyansky”, 3—“Shebekinsky”, 4—“Novooskol’sky”, 5—“Krasnogvardeisky”, 6—“Roven’sky”, 7—“Privetny”, 8—“Prudki”, 9—“Ternovka”, 10—“Bondarev”. Soil moisture regimes were studied in areas 7 and 10. Soils in areas 7, 9, and 10, according to WRB [36], are classified as Haplic and Luvic Chernozems, while the soil in area 8 is classified as Luvic Phaeozems.

The investigated sites differ from each other primarily in terms of the balance between heat and moisture. The hydrothermal coefficient (HTC) was used as a quantitative criterion for assessing this characteristic. The HTC is a climatic index that takes into account temperature and precipitation conditions during the vegetated period of the year. We calculated the HTC using Selyaninov’s formula, which takes into account the precipitation during a period with temperatures above 10 °C and the sum of the temperatures during the same period [37].

We assessed the direction and rate of afforestation within six study sites, which had a total area of 1722 km² from the wettest (point 1 in Figure 5, HTC = 1.16) to the driest

(point 6 in Figure 5, HTC = 1.00) parts of the forest-steppe. We studied the influence of shelterbelts on soils in four of the sites (from northwest to southeast), i.e., “Bondarev”, “Ternovka”, “Prudki”, and “Privetny”, and we studied the dynamics of soil moisture in the most contrasting areas in terms of the HTC, i.e., the “Bondarev” (HTC = 1.2) and “Privetny” (HTC = 0.9) sites. Soils at “Bondarev”, “Ternovka”, and “Privetny” were Haplic and Luvic Chernozems, and at the “Prudki” site they were Chernic Luvic Phaeozems. All four sites (“Bondarev”, “Ternovka”, “Prudki”, and “Privetny”) were situated on flat watersheds, and the fields were divided by long shelterbelts to ensure equal sunlight exposure on both sides. These shelterbelts were 30 m wide and consisted of multiple rows of trees aged between 50–65 years. The tree species composition varied across the sites. “Bondarev” had ash (*Fraxinus excelsior*) and elm (*Ulmus minor*), “Ternovka” had oak (*Quercus robur*), “Prudki” had oak (*Quercus robur*) and ash (*Fraxinus excelsior*), and “Privetny” had ash (*Fraxinus excelsior*), elm (*Ulmus minor*), and maple (*Acer negundo*). Traditional crops like winter wheat (*Triticum aestivum*), soybeans (*Glycine max*), corn (*Zea mays*), and sunflowers (*Helianthus annuus*) were cultivated in the fields. The soil treatment methods remained consistent across all the sites, including deep plowing (up to 30 cm) for corn and sunflowers and shallow disk harrowing for wheat and soybeans.

3. Methods

3.1. Remote Sensing and GIS Methods for Assessing Direction and Rate of Afforestation

The use of satellite information for monitoring forest vegetation is widely used today [30,32,34,35] and others. We utilized high-resolution satellite imagery in our research to objectively evaluate the alterations in forest boundaries and comprehend the direction and pace of forest establishment. We used satellite images taken by the CORONA system in the summer of 1970. These images were captured on black and white film with a spatial resolution of approximately two meters. These images, obtained from the United States Geological Survey resource, are the most detailed satellite images available for the 1960–70s period. They provided us with a unique opportunity to retrospectively assess the distribution of forested lands. Previous studies have also successfully used CORONA satellite data to analyze forest vegetation dynamics [33]. Satellite images for the end of the second decade of the 21st century (2020) included mosaic images that were obtained from the ArcGIS World Imagery software <https://www.esri.com/en-us/arcgis/products/arcgis-desktop/overview> (accessed on 7 September 2023). ArcGIS World Imagery images consist of mosaics of ultra-high-spatial-resolution (one meter) satellite imagery synthesized in natural colors. We paired satellite images of different time periods with a spatial resolution of 2 m/pixel for each area. The area of site 1 was 420.7 km², site 2 was 304.0 km², site 3 was 415.1 km², site 4 was 261.2 km², site 5 was 321.2 km², and site 6 was 313.3 km².

To accurately analyze the changes in the forest boundaries over time, we used satellite data that underwent geographical registration and geometric correction. This process involved using software such as ERDAS IMAGINE and ArcGIS to align the images from different time periods. We utilized these software packages for the geographic referencing and geometric correction of satellite data, ensuring the accuracy of the overlapping of the space images obtained in 1970 and images obtained in 2020. By doing so, we were able to effectively study the displacement of the forest boundaries. Next, we carried out detailed mapping of the forested lands, including areas under shelterbelts, in each key area using the ArcGIS software. This allowed us to prepare vector layers showing the forested lands in 1970 and 2020. With these obtained data, we created an analytical sample to quantitatively analyze the changes in the area of the forested lands over time.

In the main experimental stage, we assessed the linear rates of change in the forest boundaries on the slopes of river valleys and gully systems with different aspects (north, south, west, and east). We estimated the linear rates of change in the forest boundaries as the ratio of the total length of change over the entire analyzed period to the time during which this change (i.e., the advancement of the forest boundary) occurred. We selected forest test areas that covered slope territories corresponding to meadows or pastures where natural

forest vegetation expansion occurred. These areas were free from limitations imposed by roads, railways, human settlements, or cultivated lands, which could hinder the natural spread of forests.

For the experimental samples, we measured the distances between forest boundaries at the same study points in 1970 and 2020 using GIS. We employed the equal distance transect method (30 m) along the forest boundary to mark segments where linear forest growth occurred at each point, which was followed by automated processing of the results and calculations. The total number of measurements conducted within 6 key sections was 2086. The statistical analysis involved determining the average distance by which the forest boundaries moved and estimating the error of the average distance. We also calculated the linear rate of change in the position of the forest boundaries over a period of 10 years and compared these rates on slopes with different aspects. Additionally, we analyzed the changes that occurred in different climatic conditions in the study area.

Another important aspect of our study was mapping the density of degrading shelterbelts in the southern part of the Central Russian Upland (Belgorod Oblast). We used satellite imagery from 2020 with a spatial resolution of two meters and higher. These data were made publicly available and accessed through the ArcGIS server. We visually interpreted the satellite imagery and created a digital map showing the density of the degrading shelterbelts (Figure 6). We identified sections of shelterbelts that were completely out of use or fragmented to varying degrees and assigned separate indices to them in the attribute table. We used tools such as “line density” with a search radius of 2.5 km to construct the map (two mean distances between disappeared shelterbelts according to our observations in all study areas). We also used other tools for analyzing thematic raster images, such as “zonal statistics,” “spatial statistics,” and “analysis.”



Figure 6. Examples of satellite images showing forest plantations of varying degrees of fragmentation.

In our research, we also analyzed the correlation between the degradation of shelterbelts and the climatic characteristics within the study territory. For this purpose, we conducted a comparative analysis between the average density of degrading shelterbelts and the HTC values within their respective territories.

3.2. Soil Study and Sample Techniques. Soil Laboratory Analyses

At each of four study sites, we conducted a soil profile analysis through morphological description of deep soil pits. Two pits were dug in the center of the shelterbelts, and one pit was dug on each side of the shelterbelts in the fields at distances of 10, 30, and 60 m from their edges. Visual representations of traces left by soil fauna and burrowing animals on the front walls of the pits were documented to calculate the areas occupied by these zoogenic incursions at different depths in the soil profiles, complementing the morphological description of the soils.

Soil sampling for laboratory analysis was conducted down to a depth of 180 cm, and in deeper layers (up to a depth of four meters), a drill was used, with averaging of paired

samples extracted from two soil wells. Samples for the bulk density were collected at different depths using steel rings of known volumes with triple replication.

In addition, three transects were established at each key site, positioned perpendicular to the shelterbelts. The transects were spaced 10 m apart, with a total length of 230 m each (100 m in each field and 30 m under the shelterbelt). Sample collection (0–20 cm) was conducted at intervals of ten meters in the fields and six meters under the shelterbelts. At each sampling point, one averaged sample was collected for laboratory analysis, while two duplicate samples were taken to determine the compaction density using steel rings of known volumes.

A typical scheme illustrating the distribution of soil sampling points at key sections is shown in Figure 7.

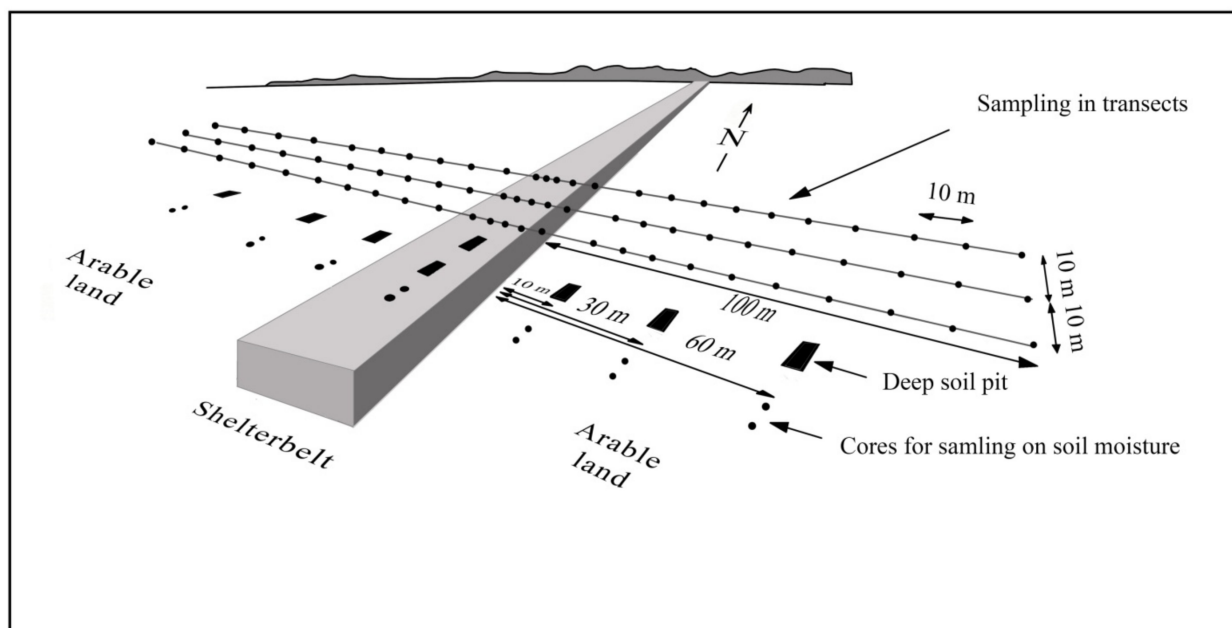


Figure 7. A typical scheme for the placement of soil profiles, drilling, and collecting soil samples for laboratory analysis at key research sites.

The laboratory analysis included determining the soil particle size distribution using the Kachinsky method (GOST 12536), the humus group composition (detection of humic and fulvic acids carbon content) using the accelerated methodology of Kononova–Belchikova [38], the pH of the soil suspension (GOST 26423-85), available phosphorus forms according to the Chirikov method (GOST 26205-91), and the composition of the salt extract (GOST 26424-85, GOST 26425-85, GOST 26426-85, GOST 26427-85, GOST 26428-85). In analyzing and interpreting the obtained data, methods of mathematical statistics were also used through the STATISTICA software package <https://www.statistica.com/en/> (accessed on 7 September 2023).

The total number of soil samples tested for bulk density was 930, and the number of samples collected for various types of laboratory analysis was 1362.

3.3. Soil Moisture Dynamics

The monitoring of soil moisture changes was conducted in two climatically contrasting plots located in the forest-steppe region. The first plot, called “Bondarev,” was in a moist forest-steppe area, while the second plot, called “Privetny,” was in an arid forest-steppe area bordering the steppe. The monitoring took place from May to October in both 2020 and 2021.

At each site, samples were collected monthly to determine the moisture content. The samples were taken from the central parts of the shelterbelts and from adjacent crop fields

at distances of 10, 30, and 60 m from the forest edges. Two duplicate wells were used at each research point, spaced 1.5 m apart, and samples were taken to a depth of two meters, layer by layer, every 20 cm. In total, 14 wells were drilled, and 140 soil samples were collected at the key sites during each observation period. A total of 3920 samples were collected over the 2 years. The soil samples from the bore cores were placed in aluminum boxes, tightly sealed with lids, and immediately weighed on special scales designed for field work, namely an OHAUS Scout SPX223 scale, with an accuracy of 0.01 g. After delivering the soil samples to the laboratory, the samples were dried in drying ovens for 8 hours at a temperature of 105 degrees Celsius and then weighed again. The soil moisture content in % by mass was calculated based on the difference in soil mass before and after drying. The average moisture values from each well were used to assess the soil moisture distribution.

In the “Bondarev” site, corn was cultivated in the field west of the shelterbelt in 2020, while winter wheat was grown in the field east of the shelterbelt. In 2021, soybeans and corn were cultivated in these fields, respectively. In the “Privetny” site, soybeans were cultivated in the fields west and east of the shelterbelt in 2020, and winter wheat was grown in 2021.

4. Results

4.1. Spatiotemporal Dynamics of Forest Vegetation

Figure 8 displays the schematic diagrams of the fragments from the six key areas studied, illustrating the changes in forestation from 1970 to 2020. The comparative analysis of the satellite images from different periods (1970–2020) revealed a significant increase in forestation across all the studied areas in the forest-steppe zone, which have varying climatic conditions. Shelterbelts played a prominent role in this increase, as indicated in Table 2 and depicted in Figures 8 and 9. Over a span of 50 years, the forestation increase ranged from 4 to 12% of the total area for the six key areas, with an overall change in forestation ranging from 14 to 22% of the total area across all areas (Table 2). Forests appeared most prominently in areas where economic activities did not hinder the afforestation, such as slopes, the bottoms of river valleys, or ravines covered with wild grasses.

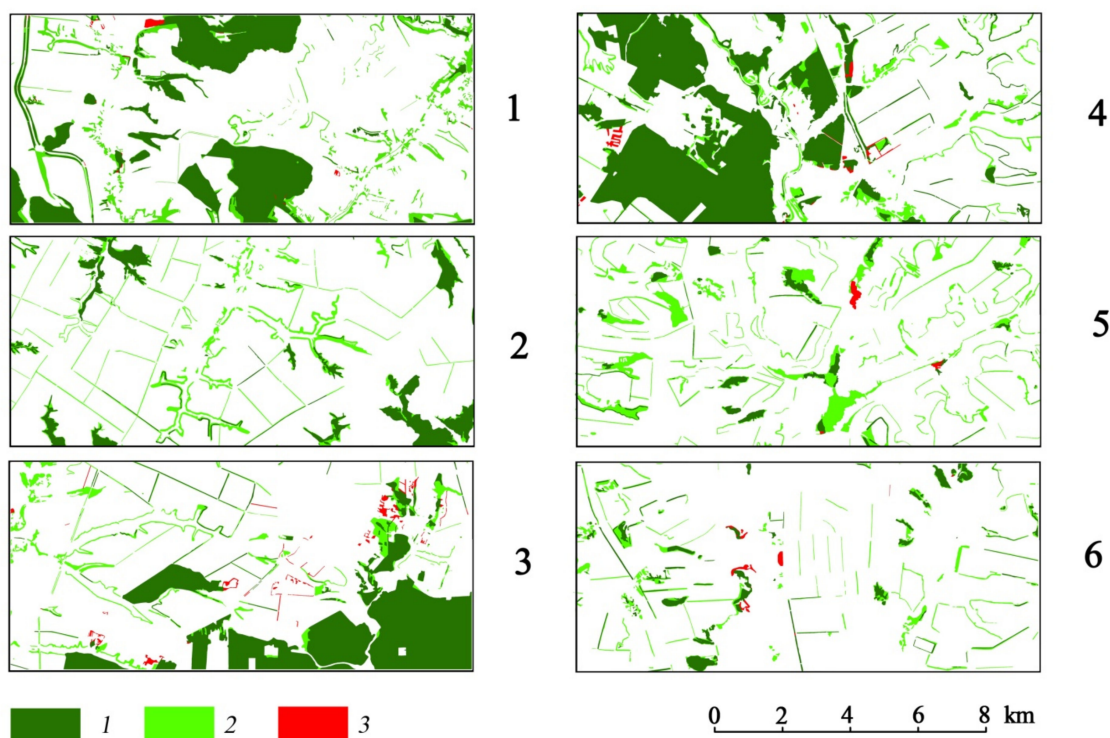


Figure 8. Fragments of cartograms depicting changes in forest cover from 1970 to 2020 at six key study sites (site numbers to the right of the panel correspond to those shown in Figure 5: 1—“Borisovskiy”,

2—“Ivnyansky”, 3—“Shebekinsky”, 4—“Novooskol’sky”, 5—“Krasnogvardeisky”, 6—“Roven’sky”). 1—Forest vegetation in 1970 and 2020; 2—forest cover areas in 2020 that emerged after 1970; 3—forest cover areas in 1970 that disappeared by 2020 (data from the authors).

Table 2. Characteristics of forest land changes assessed at key study sites during the period 1970–2020.

Site	Forest Area and Shelterbelts Area, Hectares		Forest Cover, % of Total Area	
	1970	2020	1970	2020
1	9103	13,745	21	33
2	2855	5220	9	17
3	8943	12,296	22	30
4	5829	7172	22	27
5	3195	8147	10	25
6	940	2166	3	7
Total	30,865	48,746	14	22

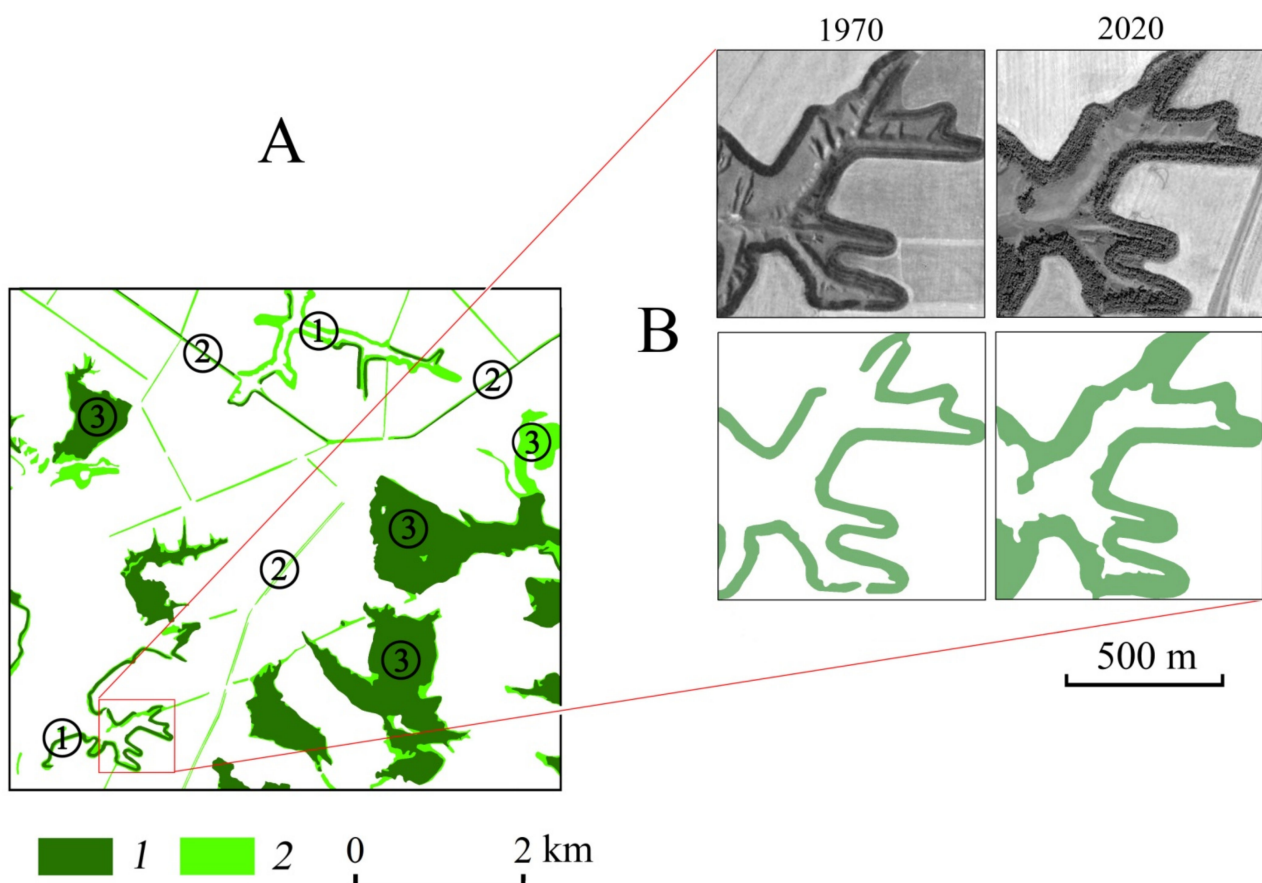


Figure 9. Fragment of key area 2 indicating different types of forested territories (A) and an example of the growth of anti-erosional shelterbelts from 1970 to 2020 (B). Legend: 1—territories covered with forest vegetation in 1970 and 2020; 2—territories where forest vegetation had appeared during the period from 1970 to 2020; 1—areas of anti-erosional shelterbelts; 2—areas of protective shelterbelts; 3—natural areas of forest vegetation.

We analyzed diagrams of the forestation changes in the six key areas and found two types of forest areas associated with an increase in forest cover. Firstly, there were

protective shelterbelts with straight lines along the flat or gentle slope watershed areas (Figures 8–10). In many places, these belts were either missing or already existed in 1970, but the trees were not tall enough (likely less than 2–3 m) to form a dense canopy visible in the satellite images. The second type was anti-erosion shelterbelts on the slopes of ravines or watersheds, separating higher arable land from lower hayfields and pastures on steeper slopes (an example is shown in Figure 9B). Many of these belts, like protective shelterbelts, were not visible in the 1970 images due to their young age and the open canopies of young trees. Unlike the protective belts on watersheds, which were constrained in their width by the surrounding cultivated fields, we mainly observed the expansion of anti-erosion shelterbelts towards hayfields and pastures down the slopes from 1970 to 2020. This often resulted in their original linear shape transforming into irregular configurations, depending on the intensity of afforestation activities on the slopes (Figures 8–10).

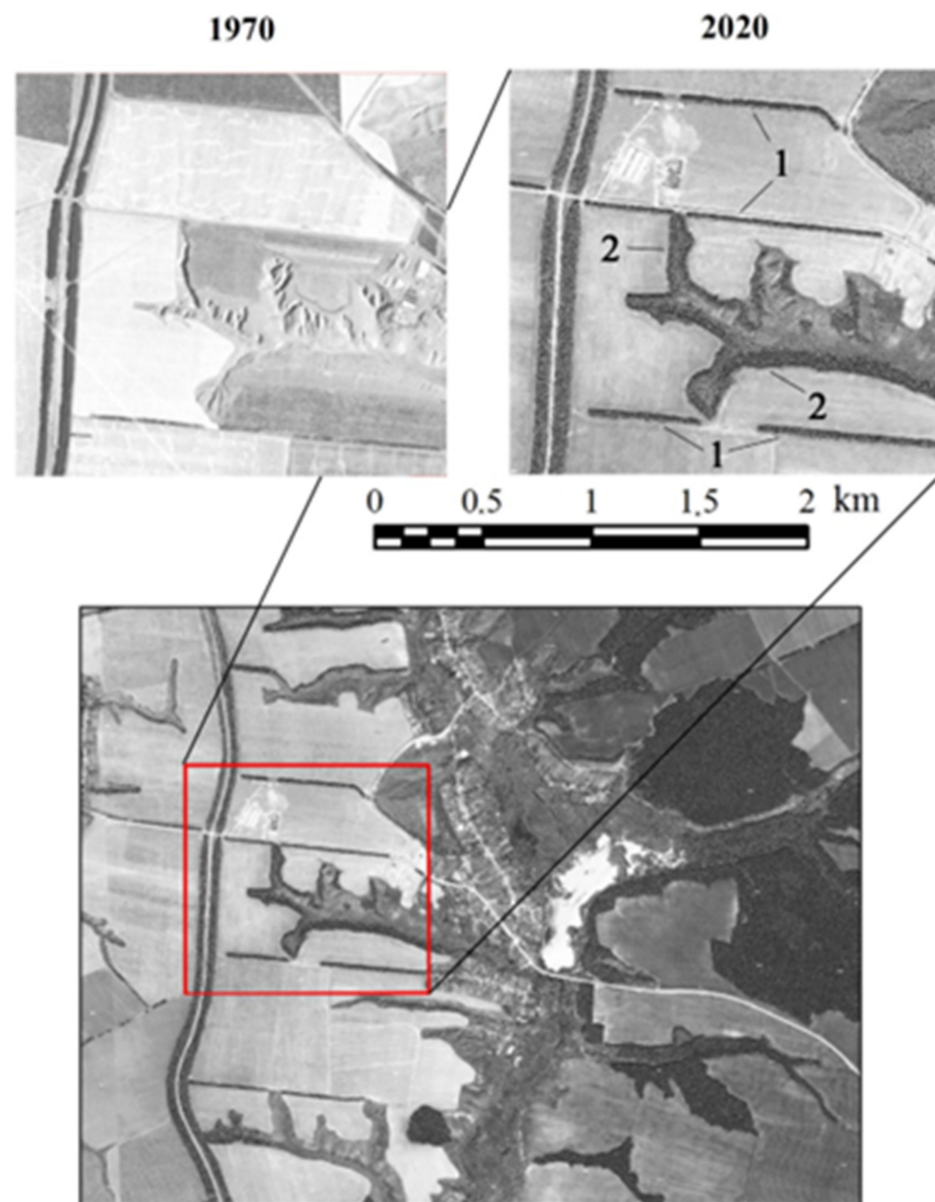


Figure 10. The above image illustrates different levels of transformation in shelterbelts based on the comparison of satellite images taken during 1970 and 2020. 1—Protective shelterbelts between arable fields with consistent contours over time; 2—anti-erosion shelterbelts near ravine slopes with significant changes in contours and increased areas (source: authors' data).

The calculations of the forest cover growth on the slopes with different aspects from 1970 to 2020 are shown in Table 3. In each area, there were no significant differences in the rates of forest growth on slopes with different aspects (Table 3). However, when considering the weighted average growth value across all six areas, there were already noticeable differences (Table 4). Specifically, the growth was faster on northern slopes compared to southern slopes and on western slopes compared to eastern slopes. Moreover, based on the weighted average value of forest growth, there was a clear tendency toward decreasing growth in areas with a more arid climate, as indicated by the decreasing values of the HTC (Table 3, Figure 11). In the more humid forest-steppe landscape, the expansion of forests onto grasslands was more intense compared to the process occurring in drier climatic conditions.

Table 3. The magnitude of linear growth of forest boundaries during the period 1970–2020, assessed at key study sites.

Site	Mean Length of Increments, m/Number of Measurements					Hydrothermal Coefficient (HTC)
	Northern Aspect	Southern Aspect	Western Aspect	Eastern Aspect	Weighted Average Value	
1	31.8 ± 1.4/117	31.5 ± 1.5/101	30.5 ± 1.7/57	28.5 ± 1.5/46	31.0 ± 1.5/321	1.16
2	20.2 ± 1.0/176	24.0 ± 0.8/109	27.8 ± 1.2/70	25.0 ± 0.8/173	23.6 ± 0.9/528	1.13
3	25.8 ± 1.0/76	26.6 ± 1.3/58	26.2 ± 1.1/75	29.7 ± 0.8/66	27.0 ± 1.0/275	1.05
4	25.3 ± 1.4/64	13.5 ± 0.7/57	22.0 ± 0.8/57	24.9 ± 0.8/85	21.9 ± 0.9/263	1.02
5	23.5 ± 1.4/121	21.5 ± 1.1/91	21.8 ± 1.5/31	14.4 ± 1.0/89	20.3 ± 1.2/332	1.01
6	18.5 ± 0.4/143	15.1 ± 0.7/86	19.3 ± 0.7/59	20.6 ± 1.5/79	18.3 ± 0.8/367	1.0
Weighted average value across 6 plots	23.5 ± 0.5/697	22.6 ± 0.5/502	25.0 ± 0.5/349	23.5 ± 0.5/538	23.5 ± 0.3/2086	1.06

Table 4. Differences in linear growth of forest boundaries on slopes with different aspects during the period 1970–2020 (based on data from Table 2).

Slope Exposure	Length of Increments of Forest Boundaries, Meters	Difference	LSD ₀₅
Northern	23.5 ± 0.5	1.1	1.41
Southern	22.6 ± 0.5		
Western	25.0 ± 0.5	1.5	1.39
Eastern	23.5 ± 0.5		

Figure 11 demonstrates that forest growth should cease when the HTC index reaches 0.78. These climatic conditions are typical of the landscapes in the southern part of the steppe zone.

During the study of the spatial–temporal changes in the shelterbelts, we also observed a noticeable trend toward decreasing shelterbelt density (length of shelterbelts per unit area), which resulted from aging and die-off, leading to the fragmentation of the shelterbelts (Figures 6 and 12).

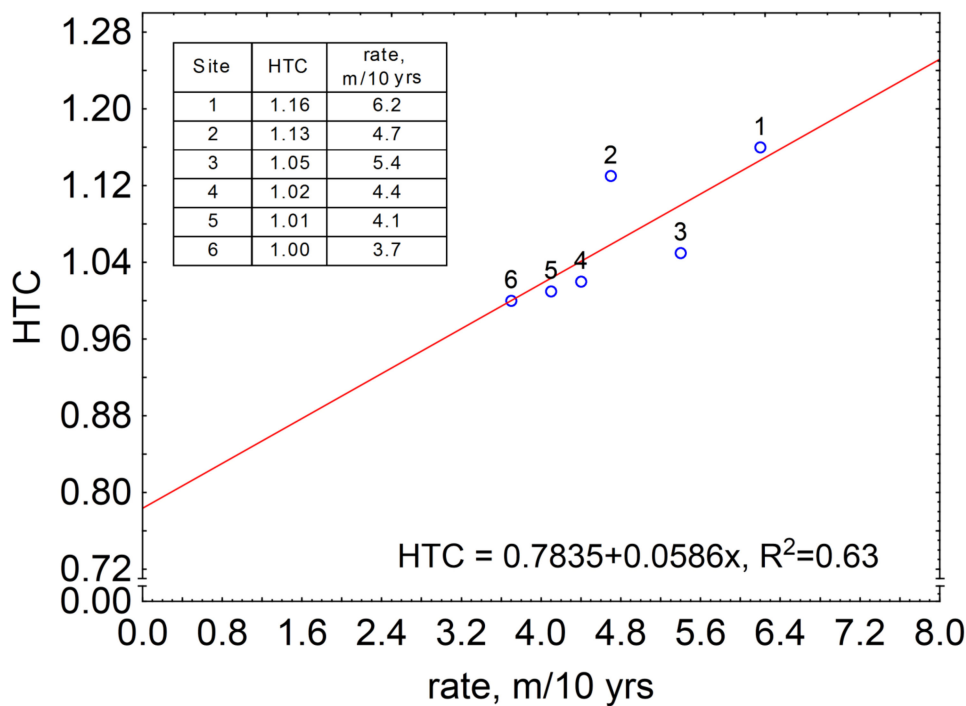


Figure 11. Linear trend of forest vegetation encroachment on grassland landscapes based on the hydrothermal coefficient in the central eastern European region. The numbers on the graph correspond to the numbers of key study sites in Figures 5 and 8 and Tables 2 and 3 (data from the authors).

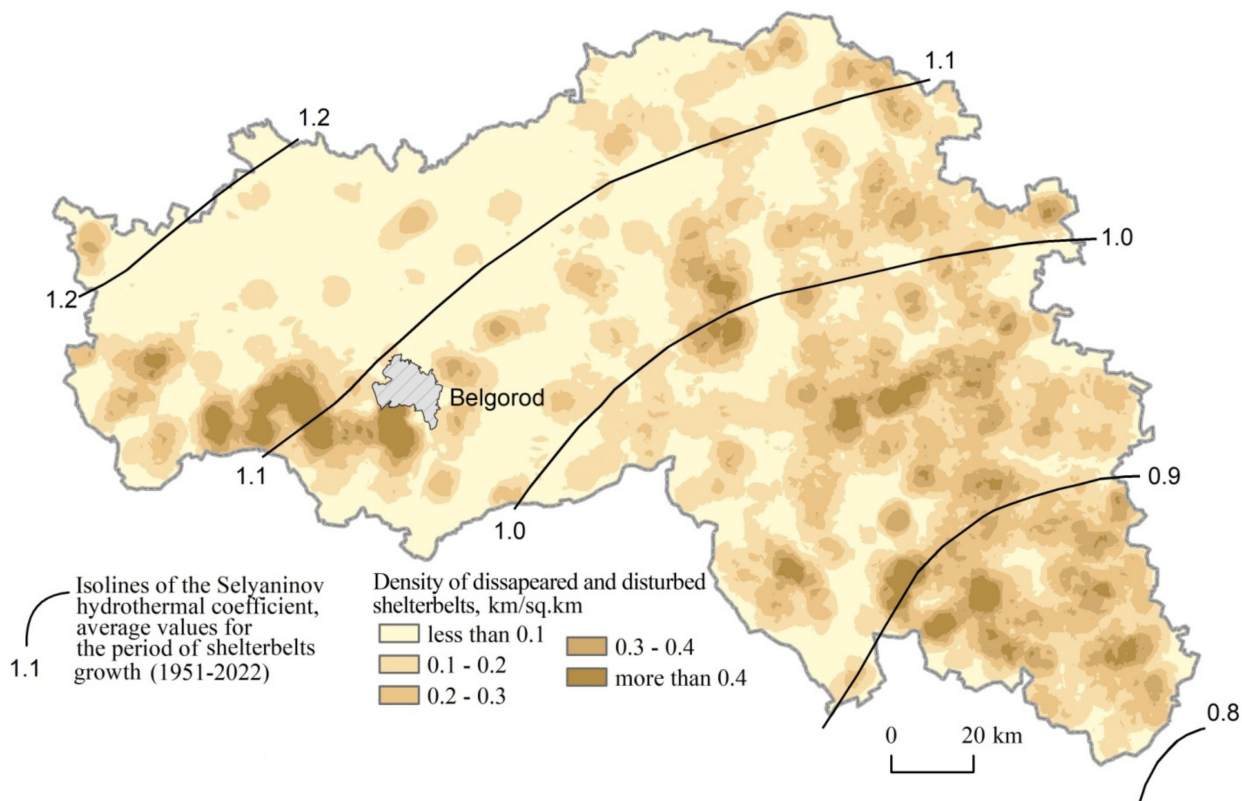


Figure 12. Density of degrading shelterbelts for all types and HTC in the Belgorod Oblast (data from the authors).

The comparative analysis of a large-scale map depicting the shelterbelt distribution in the Belgorod region during the modern period (created by the authors using satellite images) with topographic maps at a scale of 1:10,000 from the 1950s–1981s revealed a clear trend of intensifying degradation of the shelterbelts (their loss and fragmentation) as the climate became drier from northwest to southeast within the region from the forest-steppe zone towards the steppe zone (Figure 11, Table 5). This indicates a worsening of the ecological conditions for the growth of artificial forest plantations and overall forest vegetation in regions with a less humid climate. It is not accidental that, in accordance with an established regularity, a decrease in the HTC leads to a reduction in the rate of frontal advancement of forest vegetation boundaries towards grassy landscapes (Figure 11).

Table 5. Density of degrading shelterbelts in the Belgorod region for areas with different hydrothermal conditions (average values of the Selyaninov HTC over the entire period of shelterbelt growth (1951–2022)) (compiled from data in Figure 12).

HTC	0.8–0.9	0.9–1.0	1.0–1.1	1.1–1.2
Density, km/sq.km	0.23	0.17	0.13	0.10

We studied the degradation of forest vegetation under field conditions. Visually, this degradation was determined by the presence of dry trees and shrubs within the shelterbelts, especially in their central parts (Figure 13A). The drying out of tree stands over extensive areas within the shelterbelts (Figure 13B) further led to the loss of vegetation and the appearance of fragmentation within the shelterbelts (Figure 13C).



Figure 13. The (A) drying of trees in the central part of the shelterbelt, (B) drying of trees in an extensive area of the shelterbelt, and (C) formation of fragmented shelterbelt.

Thus, our research revealed two opposing processes in the changes in forest vegetation distribution over a 50-year period (from 1970 to 2020): (1) the expansion of forested areas and (2) the degradation of forest vegetation. The expansion of forested areas was attributed to agroforestry measures and favorable natural conditions. New shelterbelts emerged, and existing anti-erosional shelterbelts widened, leading to increased forested areas. The degradation of forest vegetation was caused by aging tree stands in long-established shelterbelts, their increased susceptibility to diseases over time, and the deterioration of ecological conditions due to a drier climate.

However, it is important to note that during the studied period of the spatiotemporal forest vegetation dynamics within the Belgorod region, the expansion of forested areas predominated over the degradation process. This was supported by both statistical data (Table 1) and a comparative analysis of remote sensing data from different time periods (Table 2, Figure 8).

4.2. Soil Moisture Dynamics

One important aspect of our study was examining the soil moisture dynamics the soil within the humid and dry forest-steppe regions. We selected key research sites, which are illustrated in Figure 5. The findings from our observations throughout the vegetation periods spanning two years (2020–2021) are presented in tables within this article. We believe that these unique observational data can be utilized by interested specialists for various scientific purposes (Tables 6–8).

Table 6. Soil moisture at the “Bondarev” site.

Soil Layer, cm	2020 Year						2021 Year						Mean	Standard Deviation
	Month						Month							
	5	6	7	8	9	10	5	6	7	8	9	10		
60 m to the west of the shelterbelt														
0–20	22.3	20.4	20.6	16.9	15.9	19.3	24.3	27.1	15.5	13.5	23.3	17.4	19.7	4.05
20–40	22.9	20.3	19.7	17.9	16.9	20	25.5	25.5	13.8	15	16.1	15.7	19.1	3.94
40–60	27.4	23.6	22.2	18.5	16.9	18.8	26.1	25.3	16	13.6	15.6	15.2	19.9	4.77
60–80	23	23.4	18.2	18.2	16.1	18.2	24.9	26.1	17.6	14.1	14.9	14.7	19.1	4.18
80–100	23.2	23.7	19.7	18.1	16.2	18.5	21.2	25.9	18	14	15.2	14.8	19	3.81
100–120	22	20.2	20.6	18.8	15.4	18.8	17.2	23.7	19.1	13.8	14.6	14.5	18.2	3.17
120–140	18.7	24.3	20.9	19	15	18.9	17.5	23.7	21.5	13.5	14.2	13.7	18.4	3.76
140–160	17.2	22.6	20.1	19.6	15.7	18.3	28.2	22.5	20.4	15	14.1	13.3	18.9	4.27
160–180	17.2	21	17.5	19.3	17.6	18.8	18.0	22.2	21.1	17.4	16.6	15.7	18.5	2
180–200	18.1	20.9	19.7	18.6	18.8	19.1	18.5	22	21.4	18	17.9	16.6	19.1	1.59
30 m to the west of the shelterbelt														
0–20	19.6	19.1	18.2	15.9	15.3	15.2	24.3	24.7	15.4	14.3	22.8	17.3	18.5	3.68
20–40	19.2	19.1	20.6	17.2	16.2	15.2	25.2	28.9	14.3	14.8	16.9	15.2	18.6	4.48
40–60	19.7	22.4	20.2	16.4	15	13.7	23.2	23.2	16.8	13.6	14.5	13.7	17.7	3.83
60–80	20.7	25.2	19.6	15	14.1	12.3	22.5	23.4	20.4	14.7	13.3	12.5	17.8	4.63
80–100	21.5	21.4	20.6	14.1	13.4	13.1	22.9	23.3	20.9	14.5	12.2	12.5	17.5	4.52
100–120	20.5	21.9	21.1	15	15	13.5	22	24.5	21.5	14.4	13.1	12.8	17.9	4.3
120–140	20.5	21.8	21.4	15.9	15.8	14.2	20.8	21.8	20.4	14.4	13.2	13.8	17.8	3.53
140–160	19.1	21.4	20.6	17.4	17	15.9	21.2	22.2	21.1	16.4	15.4	15.6	18.6	2.58
160–180	17.9	21.2	19.9	18.6	17.2	18.6	20.8	21.5	20.6	18.4	17.7	17.6	19.2	1.54
180–200	17.3	21.3	20.1	18.8	20.3	18	20.8	22.9	19.9	19.2	19.4	18.2	19.7	1.56

Table 6. Cont.

Soil Layer, cm	2020 Year						2021 Year						Mean	Standard Deviation
	Month						Month							
	5	6	7	8	9	10	5	6	7	8	9	10		
10 m to the west of the shelterbelt														
0–20	22.7	18.6	17.7	13.2	14.8	14	25.5	23.4	15.6	10	18.5	16.2	17.7	4.28
20–40	19.6	16.5	17.2	14.2	15.6	13.4	22.9	22.2	16.7	14.5	16.1	14.3	16.9	3.1
40–60	23.1	23.6	21	14.5	15.2	14.8	25.9	25.3	17.9	13.5	15.2	14.3	18.7	4.75
60–80	23.5	25.4	21	15.4	14.9	14	25.6	24.8	19.3	13.5	14.6	14.2	18.9	4.95
80–100	22.9	24.8	18.9	15.4	14.2	13.8	25	24.3	18.6	13.1	14.5	13.6	18.3	4.8
100–120	21.4	24.6	17.5	14.7	14.8	13.5	19.7	23.2	18.2	13.5	14.1	13.7	17.4	4
120–140	15.6	28	17.3	14.3	13.9	14	16.8	20.8	17.9	13	13.8	13.1	16.5	4.3
140–160	16	23.7	16.1	14.1	14.7	12.9	14.9	21	18	13.6	13.9	13.2	16	3.34
160–180	11.9	21.3	15.1	13.9	13.4	14.2	14.7	19.1	17.9	13.8	13.8	13.6	15.2	2.75
180–200	13.2	19.7	13.6	14.8	14.4	13.4	15.6	19.3	18.1	16.7	14.8	14.3	15.7	2.27
Shelterbelt														
0–20	27.1	20.9	17.7	14.9	13.6	12.8	25.8	24	16.9	16.2	16.7	14.9	18.5	4.84
20–40	24.8	21.3	19.2	13.6	12.2	12.3	24.6	17.5	14.4	14.4	14.1	13.6	16.8	4.59
40–60	22.9	22.4	20.3	12.7	11.9	10.7	24.4	17.6	13.8	13.9	14.2	12.8	16.5	4.82
60–80	22.4	21.5	15.3	12.2	13.3	12.4	20.5	14.6	14.5	13.4	13.9	13.9	15.7	3.63
80–100	18.7	20.1	13.9	11.9	12.4	11.5	17.2	13.3	13.7	13.6	13.8	14	14.5	2.7
100–120	17.1	19.3	13.9	12.5	12.9	12.2	25.3	14.3	14	13.4	13.7	13.5	15.2	3.77
120–140	12.3	17.1	12.7	12	13	11.7	15.9	13.7	13.3	13.3	13.9	14.5	13.6	1.59
140–160	12.2	14.9	11.1	12.1	12.7	10.5	14.4	12.5	12.9	13.4	14	13.5	12.8	1.29
160–180	12.5	12.9	11.2	12.5	11.9	11.5	15.2	12.2	13.9	12.9	12.5	13.2	12.7	1.08
180–200	13.8	13.7	13.3	13.7	12.6	11.5	15.6	12.5	15	14	12.8	13.6	13.5	1.1
10 m to the east of the shelterbelt														
0–20	16.3	15.5	19.9	15.8	15.3	12.2	22.4	17.8	11.9	12.2	16	19.3	16.2	3.25
20–40	14.4	16.8	17.1	17	14.4	12.1	20.2	19.5	12.7	14.3	14.5	14.5	15.6	2.52
40–60	13.8	20.0	21.7	18.3	13.8	12.5	24.1	20.1	17	15.1	13.4	13.3	16.9	3.86
60–80	16.1	21.9	21.1	17.6	16.4	17.7	23.2	20	16.2	15.4	13.4	13.8	17.7	3.17
80–100	17.7	20.5	17.1	16	14.6	14.2	19.5	20	16.5	15.3	14.2	13.8	16.6	2.38
100–120	18.1	20.9	13.8	15.4	13.3	13.5	18.8	18.4	16.7	14.7	13.6	13.7	15.9	2.59
120–140	16.4	19.2	13.3	14.9	13.3	11.6	17.7	17.1	16.8	13.6	12.8	13	15	2.39
140–160	14.6	17.6	13.2	14.4	13.5	11.6	16.9	16.5	16.5	13.2	12.1	13.3	14.4	1.99
160–180	13.8	17.1	14.7	13.8	13.4	12.1	16.9	17.1	16.1	15.1	13.1	13.5	14.7	1.72
180–200	13.8	15.9	14.9	13.8	13.6	11.3	16.9	15.7	16.3	16.2	13.2	14.2	14.6	1.62
30 m to the east of the shelterbelt														
0–20	21.3	16.7	20	20	18.2	19.6	25.2	23.9	14.9	13.8	22.3	18.1	19.5	3.42
20–40	19.7	18.6	21.5	18.9	22.2	22.7	25	22.5	14.1	14.9	15.1	17.5	19.4	3.51
40–60	17.1	19.4	19.3	21.4	21.5	22.9	25.5	25.4	15.2	13.6	13.9	15	19.2	4.26
60–80	18.8	19.2	21.2	20.8	20.9	21.4	25.1	26.9	15.5	12.5	13.9	14.2	19.2	4.47
80–100	19.5	19.3	17.6	20.8	20.8	20.2	25.4	25.5	16.1	13.5	14.3	15.1	19	3.92
100–120	19.7	19.8	15.3	17.5	19	18.8	20.5	22.3	19	14	15.3	14.9	18	2.59
120–140	19.6	18.9	13.5	15.7	15.1	17.7	22.9	21.8	18.7	14.5	16.7	14.8	17.5	2.98
140–160	19.1	16.9	14.3	14.6	14.2	16.7	21.8	22.9	19.8	16.8	17.5	15.8	17.5	2.85
160–180	17.8	16.7	15.4	14.6	15.5	17.2	22.1	22.5	20.3	18.9	18.4	18.1	18.1	2.52
180–200	18.3	16.8	15.7	15.3	15.7	17.9	21.8	22.7	20.3	19.7	19.1	19.1	18.5	2.4

Table 6. Cont.

Soil Layer, cm	2020 Year						2021 Year						Mean	Standard Deviation
	Month						Month							
	5	6	7	8	9	10	5	6	7	8	9	10		
60 m to the east of the shelterbelt														
0–20	19.8	15.4	18.6	19.7	20.9	16.1	20.7	23.2	13.6	14.3	20.8	19.2	18.5	2.99
20–40	19.3	18.7	17.3	20.8	19.1	19.6	22.7	21.6	13.9	13.9	14.9	15	18.1	3.04
40–60	19	20.7	21.2	21.3	20.3	16.6	24.3	22.3	14.1	13.3	13.8	13.7	18.4	3.89
60–80	18.2	19.9	19.9	19	17	16.5	25.2	22.8	12.9	12.6	13.5	13	17.5	4.09
80–100	19	19.4	19.1	16.5	15.1	16.3	24.2	22.7	12.8	12.2	13.1	13.1	17	3.98
100–120	20.3	19.6	15.9	15.7	14.6	16.9	23.9	20.8	16.2	12.5	14	13.7	17	3.43
120–140	20.4	18.8	14.1	14.6	14.4	17.4	22.8	20.5	18.2	14.7	14.7	13.8	17	3.08
140–160	18.9	18.2	13.7	13.7	14.7	15	22.3	20.2	19.9	15.9	16.4	15.8	17.1	2.79
160–180	15.2	17.8	13.3	15	15.6	16.2	21.4	23.3	20.7	18.7	18.5	17.2	17.7	2.95
180–200	17	18.7	13.3	15.9	16.4	14.5	21.5	20.1	19.8	20.3	19.2	18	17.9	2.51

Table 7. Soil moisture at the “Privetny” site.

Soil Layer, cm	2020 Year						2021 Year						Mean	Standard Deviation
	Month						Month							
	5	6	7	8	9	10	5	6	7	8	9	10		
60 m to the west of the shelterbelt														
0–20	24.1	22.5	20.5	20.5	19.9	17	20.8	20.8	16.6	23.2	20.8	21.3	20.7	2.19
20–40	23.6	23.3	20.4	18.1	23.6	19.2	23.4	22.1	16.3	21.2	16.9	17.3	20.5	2.81
40–60	23.3	21.2	18.1	16.2	20.5	17.1	24.8	22.3	16.8	20.4	17.1	16.3	19.5	2.97
60–80	24.9	20.2	17.4	15	17.2	16.3	24	21.3	16.2	19.3	17.3	17.0	18.8	3.16
80–100	21.9	19.2	16.2	15.2	15.7	15.2	24.2	20	15.8	18.3	17.1	15.9	17.9	2.91
100–120	20.9	19.8	15.4	13.5	13.5	14.3	22.6	20.2	15.5	18.1	15.6	16.4	17.2	3.08
120–140	17.2	20.1	16.2	13.7	15.7	14.3	21.2	19.6	16.7	18.7	16.8	17.2	17.3	2.27
140–160	18.5	19	18.3	14.4	16.1	16	21.3	20.7	17.8	19.8	17.0	18.9	18.1	2.02
160–180	16.9	18.3	19.1	13.3	18.9	15.4	21.3	20.6	18	20.2	16.9	19.0	18.2	2.27
180–200	15.1	19.2	19.6	16.3	18.1	16.5	19.1	21.8	19.3	20.3	18.6	19.7	18.6	1.87
30 m to the west of the shelterbelt														
0–20	24.7	27.3	23.2	19.9	20	18.4	23.8	23.2	18.2	24.2	22	23.3	22.4	2.74
20–40	25.8	26.8	25.5	17.8	22.4	21.8	24	25.7	18	20.6	17.2	19.9	22.1	3.44
40–60	21.8	24.2	23.3	17	19.4	19.1	25.6	23.6	17.2	18.9	18.9	19.2	20.7	2.89
60–80	23.4	23.3	21	15.2	18	17	26	23.4	17	18.3	18.9	18.7	20	3.33
80–100	20.7	22	18	16.8	18.5	17.4	25.6	22.8	16.2	17.2	18.7	17.7	19.3	2.87
100–120	20.8	25.4	17	16.4	15.7	16.6	24.4	20.7	16.4	17	17.8	18.2	18.9	3.25
120–140	19.2	21.7	24.5	15.9	17.7	17.8	20.9	21.3	17.6	18.2	18.9	18	19.3	2.37
140–160	17.7	21.2	18.5	16.1	18.3	17.8	20.2	21.4	18.3	19.7	18.9	18.5	18.9	1.52
160–180	18.1	18.7	18.7	17.8	15.9	17.8	20.5	21.8	19.8	20.7	19.9	19	19.1	1.59
180–200	16	20.1	18.7	15.9	17.2	16.7	20	21.7	19.3	20.6	19.6	19.8	18.8	1.9

Table 7. Cont.

Soil Layer, cm	2020 Year						2021 Year						Mean	Standard Deviation
	Month						Month							
	5	6	7	8	9	10	5	6	7	8	9	10		
10 m to the west of the shelterbelt														
0–20	26	28.8	24.6	16.5	19.6	19.6	24.9	19.9	18.1	23.3	19.7	22.3	21.9	3.64
20–40	26.2	28.8	26.3	19.7	15.8	20.9	26.5	22	20.1	23.7	18.3	20.7	22.4	3.9
40–60	25.7	25.9	18.7	21.4	21.1	17.8	27.3	21.3	18.2	22	20.7	20.8	21.7	3.07
60–80	28.6	25.6	17.8	24.7	19.3	16.4	27.6	22.1	18.3	21.2	20.6	21	21.9	3.92
80–100	24.3	25.6	17.2	21.7	16.7	16.9	26.4	21.7	18.2	20.4	19	20.4	20.7	3.35
100–120	21.8	24.1	17.6	19.9	18.5	17.7	25	22.1	17.8	18.9	18.9	19.3	20.1	2.53
120–140	20.8	23.1	18	18.4	18.5	16.9	22.4	20.7	19.6	19.1	18.8	18.2	19.5	1.86
140–160	19.6	22	18.5	18.7	18.9	17.9	20.8	20.6	18.5	20	18.7	18.4	19.4	1.23
160–180	20.9	22.1	18.4	19.3	19.1	18.1	20.7	20.8	19.3	20.3	19.2	19.4	19.8	1.16
180–200	19.2	22.1	18.3	19.6	19.3	18.2	21.3	20.6	20.3	21.2	19.1	19.6	19.9	1.22
Shelterbelt														
0–20	24.5	20.3	17.1	16.9	13.9	17.9	31.5	28.7	17.6	17.8	17	17.6	20.1	5.34
20–40	23.7	21.7	19	16.9	14.3	15.5	32.5	23.8	17.4	17.5	17	17.2	19.7	5.04
40–60	23.7	21.6	18.7	16.1	15.6	14.9	31.3	23.6	17.3	17.4	18.7	18.2	19.8	4.65
60–80	22.8	20.1	16.5	15.5	15.8	14.8	28.5	22.2	17.2	17.3	17.7	17.6	18.8	3.95
80–100	21.3	18.8	16.2	16	14.4	15.1	27.2	22.1	17	17.2	17.3	16.7	18.3	3.62
100–120	16.7	17.6	14.5	15	14.5	15.1	27.3	20.3	15.9	16.7	16.8	16.5	17.2	3.55
120–140	15.2	16.3	14.5	14.5	13.5	13.9	27.8	17.5	15.8	16.1	17.1	15.4	16.5	3.77
140–160	14.1	15.7	13.4	14.2	13.1	12.6	16.3	15.5	14.5	15.9	15.7	15.4	14.7	1.22
160–180	13.6	15.7	14	14.8	12.7	13.4	14.9	15.5	13.6	15.9	15	16.5	14.6	1.17
180–200	9.8	15.5	13.9	13.6	12.6	12.9	15.2	13.4	14	16.5	14.8	16	14	1.81
10 m to the east of the shelterbelt														
0–20	28.1	22.3	22.9	19.7	20.3	19.1	23.6	21.6	21.6	20.1	21.2	24.5	22.1	2.49
20–40	28.3	22.2	20.1	17.9	17.3	21.9	25.5	22.9	20.5	19	19.9	21.9	21.4	3.12
40–60	28.6	21.9	18.1	17.1	18	19.3	26.4	24	20.5	19.5	20.9	20.4	21.2	3.5
60–80	28.1	21.4	17.6	16.7	17.7	16.5	27.2	23.5	19.4	19.4	19.3	19.5	20.5	3.86
80–100	27.6	21.5	17.1	15.8	16	16.3	27.1	23.6	18.8	18.8	19	19.1	20.1	4.09
100–120	25.9	22.3	16.7	15	17.3	15.9	24.7	23.7	18	16.7	18.1	19.1	19.5	3.71
120–140	23.2	23.2	16.2	14.8	15.1	14.4	23.7	21.7	19	16.8	18.3	18.9	18.8	3.46
140–160	20.8	21.7	16.8	15.8	15.4	15.6	22.5	22.6	20.3	18.6	19.6	19.2	19.1	2.65
160–180	19.8	20.2	17.4	15.3	16.7	17.7	22.6	22.5	21.4	19.8	19.8	20.2	19.5	2.27
180–200	18.6	19.6	17	15.4	14.7	16.5	23	22.5	21.3	19	20.6	21.3	19.1	2.75

Table 7. Cont.

Soil Layer, cm	2020 Year						2021 Year						Mean	Standard Deviation
	Month						Month							
	5	6	7	8	9	10	5	6	7	8	9	10		
30 m to the east of the shelterbelt														
0–20	25.7	25.2	21.3	20.4	19.3	17.5	23	17.8	21.3	22.9	23.3	22.6	21.7	2.62
20–40	28.6	23.4	20.5	21.2	21	21.2	24.8	19.4	21.6	22.8	20.6	19	22	2.64
40–60	28.4	22.5	17.4	17.3	18.8	17.8	25.5	20.1	19.3	17	19.1	18.9	20.2	3.55
60–80	27	20.7	16.1	17.2	17.6	17.1	27.5	20.2	19.3	16.5	18.8	18.3	19.7	38
80–100	25.2	21.1	15.5	16.1	15.9	15.6	27.9	20.1	18.4	16.4	18.3	18	19	3.97
100–120	24.9	21.9	15.7	15.6	15	14.4	25.1	20.3	17	15.3	16.9	16.7	18.2	3.84
120–140	22.1	20.8	14.4	16.6	10.8	14.9	22.3	18.1	17.4	16.1	18.1	16.6	17.4	3.31
140–160	20.5	21.7	16.2	18.4	17.3	17.8	21.9	19.8	20.7	17.4	18.7	17.9	19	1.86
160–180	20.5	21.3	18.1	18.3	18.9	18.5	22	19.9	20.9	18.8	20.4	20.3	19.8	1.28
180–200	20.1	20.6	18	17.4	17.6	18.2	21.9	21	21.1	18.6	20.5	21.2	19.7	1.61
60 m to the east of the shelterbelt														
0–20	26.2	20.6	24.8	22.7	20.9	17.7	21.4	18.4	20.1	21.6	21.1	22.4	21.5	2.39
20–40	28.8	20.7	24.7	20.4	19.1	18.9	22.1	20	20.2	17.5	19.1	19.7	20.9	3.06
40–60	28.6	20	20.2	19.4	16.8	16.9	25.7	21.1	19.2	16.9	18.7	18.1	20.1	3.61
60–80	26.3	18.5	17.9	18.1	16.8	16.5	27	19.9	19.5	17	18.3	18.9	19.6	3.47
80–100	25.2	19.3	17.4	16.7	16.5	16.5	24.9	21	19.2	16.6	17.8	18.9	19.2	3.08
100–120	21.7	19.2	16.4	16.1	15.4	15.8	24.9	22.7	18.9	16.2	16.1	18.6	18.5	3.13
120–140	21.6	20.7	16.7	17	17.4	16.1	22.4	20.3	18.4	15.9	16.2	18.5	18.4	2.28
140–160	20.8	20.1	17.5	17.7	16.9	16.1	20.3	20.3	20.6	17.9	17.9	20.4	18.9	1.69
160–180	20	18.9	19	18.7	17.1	15.6	22	20.4	21.9	19.7	18.5	19.9	19.3	1.81
180–200	19.4	18.5	18.8	18.7	17.8	16.6	21	21.1	21.7	20.4	19.3	20.9	19.5	1.53

Table 8. Average soil moisture values (% of soil mass) during the vegetation periods (May–October) of 2020–2021 within the key research sites “Bondarev” and “Privetny”.

Soil Layer, cm	Observation Site						
	Arable Land to the West of the Shelterbelt			Shelterbelt	Arable Land to the East of the Shelterbelt		
	Average 10–60 m	Average 10–60 m	10-m		10-m	Average 10–60 m	Average 10–60 m
Bondarev site							
0–20	18.6	18.1	17.7	18.5	16.2	17.8	18.1
20–40	18.2	17.8	16.9	16.8	15.6	17.5	17.7
40–60	18.8	18.2	18.7	16.5	16.9	18.0	18.2
60–80	18.6	18.4	18.9	15.7	17.7	18.4	18.1
80–100	18.3	17.9	18.3	14.5	16.6	17.8	17.5
100–120	17.8	17.7	17.4	15.2	15.9	17.0	17.0
120–140	17.6	17.2	16.5	13.6	15	16.2	16.5
140–160	17.8	17.3	16	12.8	14.4	16.0	16.3
160–180	17.6	17.2	15.2	12.7	14.7	16.4	16.8
180–200	18.2	17.7	15.7	13.5	14.6	16.5	17.0

Table 8. Cont.

Soil Layer, cm	Observation Site						
	Arable Land to the West of the Shelterbelt			Shelterbelt	Arable Land to the East of the Shelterbelt		
	Average 10–60 m	Average 10–60 m	10-m		10-m	Average 10–60 m	Average 10–60 m
Privetny site							
0–20	21.7	22.2	21.9	20.1	22.1	21.9	21.7
20–40	21.7	22.2	22.4	19.7	21.4	21.7	21.4
40–60	20.6	21.2	21.7	19.8	21.2	20.7	20.5
60–80	20.2	21.0	21.9	18.8	20.5	20.1	19.9
80–100	19.3	20	20.7	18.3	20.1	19.5	19.4
100–120	18.7	19.5	20.1	17.2	19.5	18.8	18.7
120–140	18.7	19.4	19.5	16.5	18.8	18.1	18.2
140–160	18.8	19.2	19.4	14.7	19.1	19.1	19.0
160–180	19.0	19.4	19.8	14.6	19.5	19.6	19.5
180–200	19.1	19.4	19.9	14	19.1	19.4	19.4

According to Roshydromet, the moisture conditions during the active vegetation periods in 2020–2021 were unstable, which is a common characteristic of the current stage of climate change noted in the region. At the beginning of the vegetated period during spring 2020, the Chernozems in the agricultural landscapes of our research area (southern part of the forest-steppe zone of the Central Russian Upland) had sufficient storage of productive soil moisture. However, starting in June, when the weather became hot and predominantly dry, drought occurred in the study areas. The available moisture storage within the meter-deep layer of Chernozems decreased to 22% of the field water capacity. Due to limited rainfall and the hot, dry weather conditions, significant soil moisture losses and severe drying of the upper soil horizons were observed in August and September. The length of the period without effective precipitation (more than 5 mm) in hot dry years up to 10 October ranged from 48 to 71 days. “Agricultural drought”, a dangerous atmospheric phenomenon, occurred in the fields during September and October. The available moisture storage ranged from 41 mm in the 0–100 cm layer to 1–5 mm in the 0–20 cm layer in the Chernozems of the southern forest-steppe zone.

In May 2021, there was an excess of precipitation. The monthly amounts ranged from 70–92 mm (160–209% above the normal). June was characterized by predominantly warm weather with unevenly distributed rainfall. In the southern part of the Belgorod region, from 20–26 June, there was a dangerous agrometeorological phenomenon called the “Sukhovoy” (dry wind).

July was characterized by hot weather and highly uneven rainfall distribution. The rains were sporadic and heavy. In the meter-deep layer of Chernozems, there was 130–140 mm of available moisture, and in the ploughed soil layer, there was 8–13 mm. By the end of July, the agrometeorological conditions worsened with the occurrence of dry wind phenomena, dry winds, atmospheric drought, and a prolonged absence of effective precipitation. Against the backdrop of hot and dry weather, the soil experienced moisture loss, particularly in the upper soil layers. In September and October, the moisture content in the meter-deep soil layer remained satisfactory (90–136 mm), and in the 0–20 cm layer of ploughed Chernozems, the available moisture ranged from 10–30 mm.

The analysis of two years’ worth of observations for changes in soil moisture within the influence zones (Tables 6–8) enabled us to draw several key conclusions.

In general, the moisture content in the soils within the “Privetny” area, located in the arid conditions of the forest-steppe zone (HTC = 0.9), was higher compared to the soils of the “Bondarev” area, located in the more humid conditions of the forest-steppe (HTC = 1.2). The main reason for the observed differences was the higher clay-like texture

of the soils in the “Privetny” area (clays retain more capillary and film moisture, increasing the overall soil moisture percentage); in the 0–20 cm soil layer, the clay fraction with a size < 0.01 mm constituted 63–79%, and in the 180–200 cm layer, it ranged from 66–85%. Similar soil indicators in the “Bondarev” area of the humid forest-steppe were 55–62% and 64–69%, respectively.

The second important conclusion was the formation of decreased soil moisture content zones in the soil under the shelterbelts (Tables 6–8, Figure 14). This was due to the effect of root desiccation by trees, which extract the necessary moisture from a greater depth much more intensively than the roots of cultivated plants.

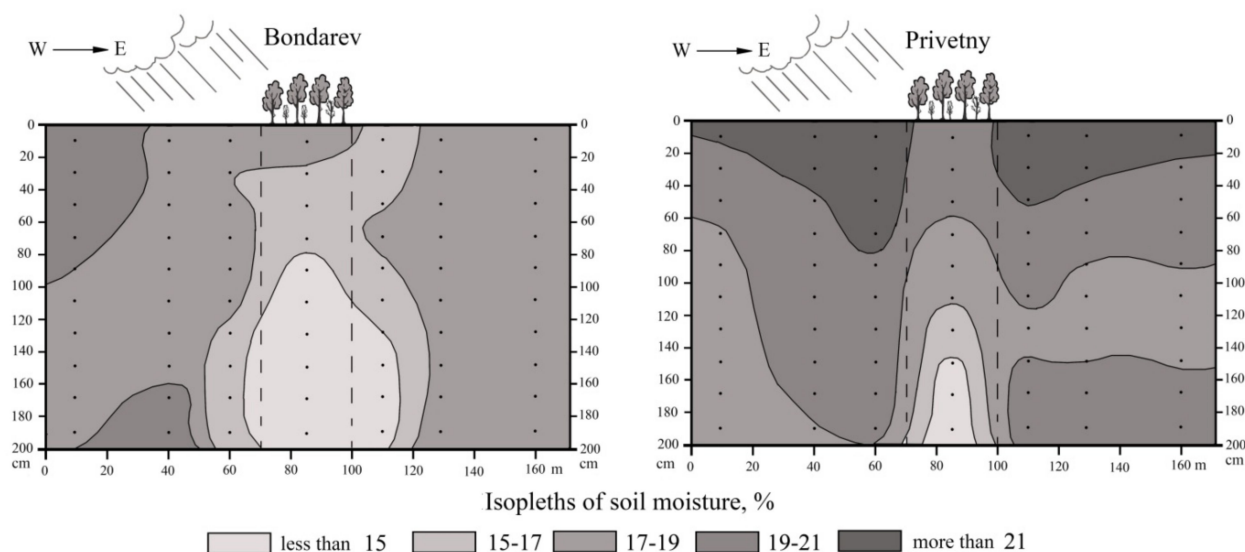


Figure 14. Soil moisture isopleths within the two studied sites (average values for the vegetation periods of 2020–2021) (data from the authors).

The third conclusion was based on the analysis of the standard deviations of the soil moisture content in different locations and at different depths within each plot. In the 0–60 cm soil layer under the shelterbelts on two plots, a higher variability in the moisture content during vegetation periods was found compared to arable soils (Tables 6 and 7). This indicates a higher degree of uniformity in the use of moisture by the roots of cultivated plants compared to the upper layer of the root systems of woody vegetation. However, in the 140–200 cm soil layer, the opposite trend was observed: the standard deviations of the moisture content in the soil under the shelterbelts was lower than in the same soil layer of arable soils (Tables 6 and 7). This can be explained by the fact that at greater depths, the roots of cultivated plants are no longer able to actively utilize soil moisture due to their physiology, the content of which can vary according to changes in weather conditions (as well as due to the penetration of atmospheric precipitation to a greater depth during the post-harvest period when moisture retention by the roots of cultivated plants is absent).

On the other hand, woody vegetation, regardless of weather changes (rainy or dry) during the vegetation periods continued to permanently and actively use deep soil moisture.

One of the most important conclusions arising from the analysis of the observation results was the recognition of more intensive soil moisture accumulation in fields located west of the shelterbelts compared to fields located east of them (Table 8, Figure 14).

This trend was most pronounced in the 10 m zone of agricultural fields adjacent to the shelterbelts (Table 8).

In the more humid forest-steppe, differences were observed in zones up to 60 m away from the edge of the shelterbelts (plot “Bondarev”), while in drier forest-steppe conditions with less atmospheric precipitation, these differences were seen in a narrower 30 m space of arable lands on both sides of the shelterbelt edges (plot “Privetny”) (Table 8).

The explanation for this pattern is that the eastern European center is in an area where air masses predominantly move from the west [39]. Therefore, agricultural fields on the windward side of the shelterbelts receive more moisture compared to the soils on the leeward sides. In addition, the tall (20–25 m) wall of trees in the shelterbelts forms a wind and rain shadow on the arable lands to the east of the shelterbelts.

For the same reason, due to uneven moistening of the western and eastern slopes of watersheds and ravines, in our opinion, a more intensive linear growth of woody vegetation was established on the western slopes compared to the eastern slopes (Tables 3 and 4).

4.3. The Influence of Afforestation on Soil Properties

The next aspect of the conducted research was the study of various morphological and chemical properties of the soils under the shelterbelts and on arable lands at different distances from the shelterbelts. Studies have shown that tree roots extend more than 10 m from the edge of the shelterbelts. This was found universally in the soil research sites (sites 7–10 in Figure 5). As an example, Figure 15 shows a profile of Chernozem soil investigated on arable land 10 m from the edge of the shelterbelt in the “Bondarev” plot with the presence of tree roots on the profile walls.

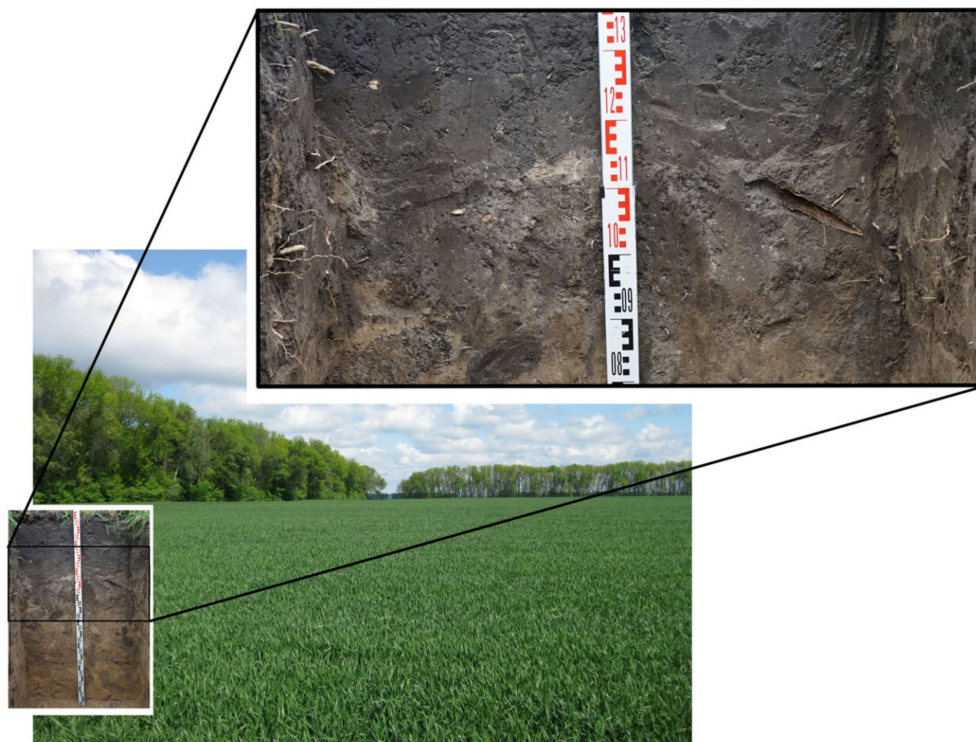


Figure 15. Living and dead tree roots in the soil profile wall at 10 m from the edge of the shelterbelt in the “Bondarev” site.

The result of tree root extension into the arable fields in different directions from the shelterbelts was the lateral uptake of substances from arable soils into the shelterbelt soils by these roots. One example of such uptake is the spatial profile of mobile phosphorus distribution within the soils, which was studied in the “Ternovka” site (Figure 16).

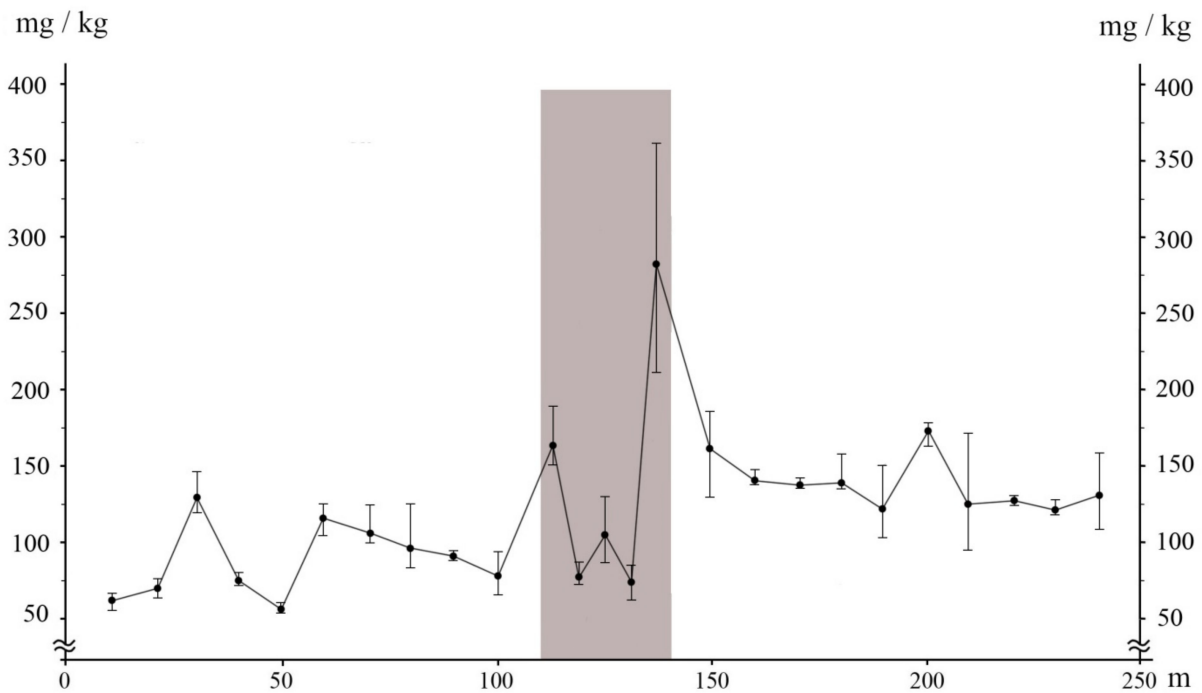


Figure 16. Spatial trend of change in the content of labile phosphorus in the 0–20 cm soil layer along the transect line at the “Ternovka” site (the gray shading represents the shelterbelt).

Trees absorb phosphorus from mineral fertilizers in fields, storing it in their roots. Later, when leaves and branches fall, the phosphorus is accumulated in the soil. Over time, this accumulation increases in the edge zones of the shelterbelts, forming distinctive soil geochemical anomalies. This process is controlled by the amount of mineral fertilizer applied to the fields: the higher the doses of fertilizer applied, the more pronounced the accumulation of plant nutrients in the peripheral areas of the shelterbelts.

In addition to the lateral uptake of substances, tree roots under the shelterbelts perform a radial (vertical) uptake of substances, indicated by the accumulation of easily soluble salts and, particularly, sodium in the parent rocks beneath the shelterbelts (Figure 17).

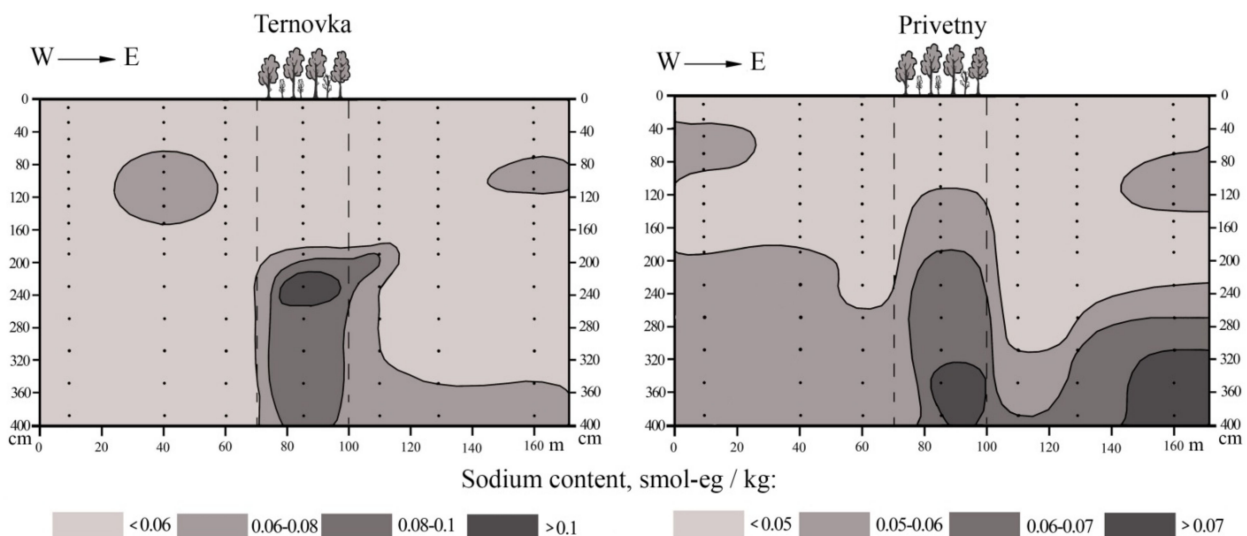


Figure 17. Sodium content in soil saline extract at “Ternovka” and “Privetny” sites.

The analysis of the spatial changes in the aforementioned soil properties and some others revealed the formation of striped microstructures in the soil cover under the shel-

terbelts and adjacent arable land areas, or the linear soil ecological zones, if these linear sections are viewed in terms of the unique ecological conditions that affect vegetation and the overall biota, including soil-dwelling animal populations.

Certain soil properties (such as pH and humus group composition) during the development of the shelterbelts led to the formation of two types of zones: the central zone under the shelterbelts, where the soil is acidified and the humus group composition changes with increased fulvic acid content in the 0–20 cm layer, and the arable land zone on both sides of the shelterbelts, showing a homogeneous distribution of pH and the ratio of C humic acids to C fulvic acids (Figure 18A,B).

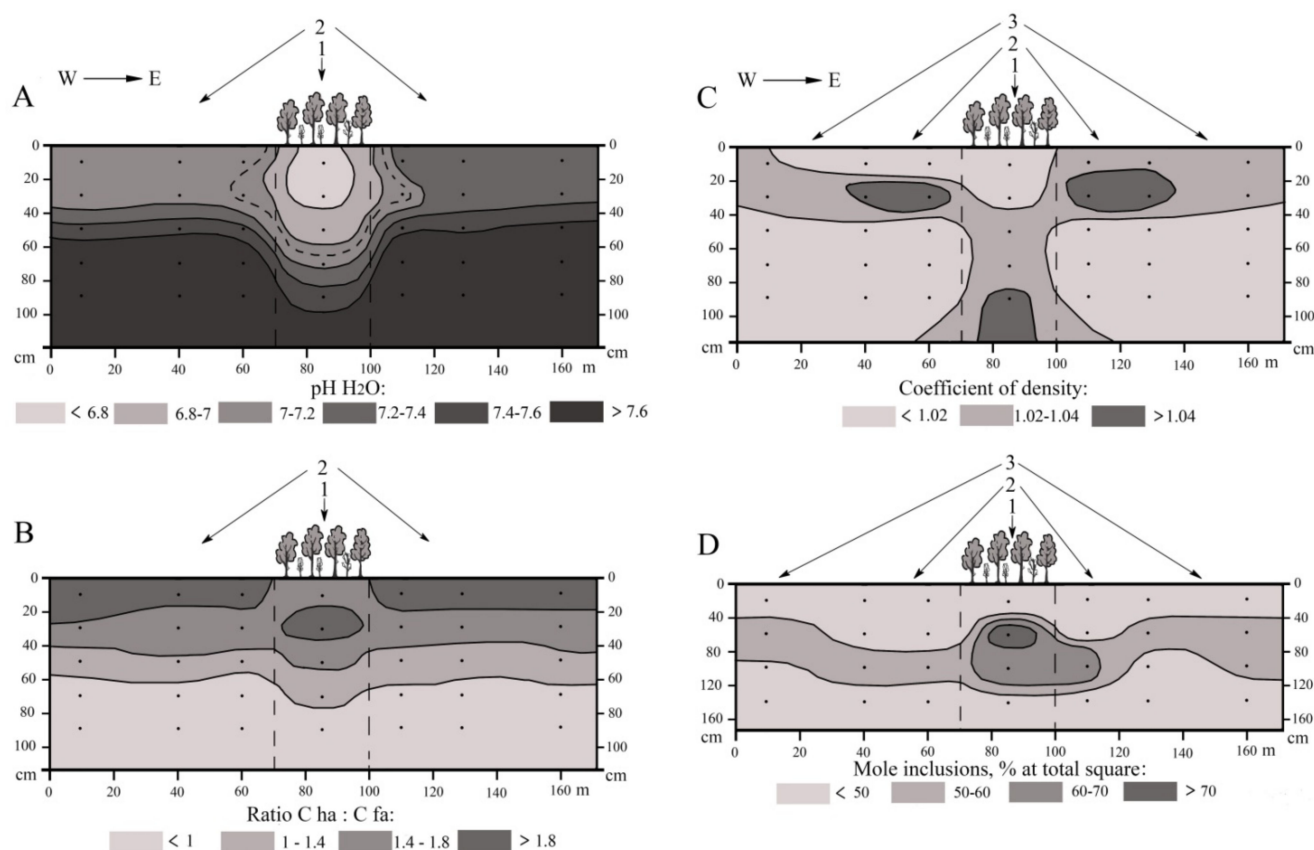


Figure 18. Different spatial couplings of soil microstructure types or soil ecological zones: for diagrams (A,B) (pH of water, ratio of humic and fulvic acid carbon contents (Cha: Cfa))—two types; in diagrams (C,D) (coefficient of density, mole inclusion areas)—three types.

The distribution of other properties, such as the compaction coefficient (resulting from the frequent passage of machinery along the field boundaries adjacent to the shelterbelts) and the area occupied by the burrows of blind mole rats, clearly indicates the formation of three types of soil ecological zones: a central zone with environmentally favorable conditions under the shelterbelts, a depression zone within a 30 m distance from the edge of the shelterbelts on the arable land, and a third zone of soil improvement, extending to the more remote part of the arable land away from the shelterbelts (Figure 18C,D).

5. Discussion

This study found that anti-erosion shelterbelts, which spread down slopes towards grasslands like meadows and pastures, were one of the main factors causing the increasing forest area in the forest-steppe region of central eastern Europe. The observed growth of forested areas from 1970 to 2020, among other factors, was also influenced by favorable climatic conditions. Climate humidification, documented in the late 20th and early 21st centuries, has been discussed in our previous works [40], and the link between forest

growth and climate humidification has been established not only in eastern Europe but also in the United States [40]. This climate characteristic is visually illustrated by the meteorological data from the oldest meteorological station in the studied region (Belgorod Oblast)—Bogoroditskoye-Fenino (instrumental weather observations have been conducted at the station since 1890) (Figure 19).

The observed increase in forested areas is likely a universal trend during the current Holocene climate period. This has been discussed in numerous publications focusing on paleogeographical reconstructions of natural environments in the forest-steppe zone, both in Russia [41–43] and in other countries [44–46]. Some studies provide evidence for a drier climate during the Bronze Age, when grasslands expanded further north and forests were limited to river valleys and ravine bottoms [47–49].

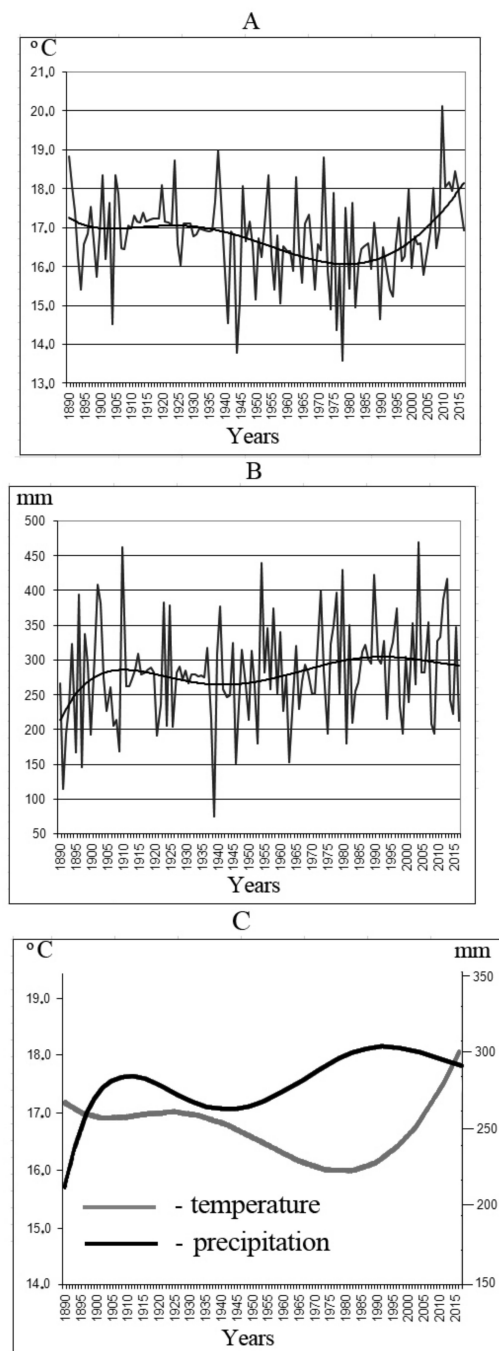


Figure 19. Trends in meteorological indicators at the Bogoroditskoye-Fenino station: (A)—average temperatures for the “May–September” period with a sixth-order polynomial, (B)—average amounts

of atmospheric precipitation for the “May–September” period with a sixth-order polynomial, (C)—polynomial smoothing of temperature and precipitation trends for the “May–September” period (sixth-order polynomials) (based on data from [50]).

The calculated forest vegetation growth rates (mainly the edge zones of anti-erosion shelterbelts) from 1970 to 2020 can contribute to reconstructions for late Holocene forest-steppe landscape formation. They reflect climate moistening, forest expansion into steppe areas, and the movement of local forested areas from river valleys and ravine slopes to watersheds.

This study provides evidence for a link between the linear growth rate of forest boundaries and climatic conditions. There is a linear relationship between the decrease in forest area growth rates and the increasing aridity of the climate (decreasing values of the moisture condition index). This corresponds to the intensification of degradation processes caused by increased fragmentation of mature shelterbelts.

The important finding in this work was the higher soil moisture in the fields west of the south-oriented shelterbelts compared to the soils in the fields east of the belts. We did not find similar conclusions in the works of other authors. Of course, further research on new sites will be needed to confirm this trend. However, in our opinion, the plausibility of this conclusion is consistent with the significant differences we observed in the linear growth of forest boundaries on slopes with different aspects. On the windward western slopes, which receive more precipitation, the intensity of forest encroachment onto grassland landscapes was significantly higher compared to the process on the slopes with an eastern aspect (Tables 3 and 4).

Our study also highlights the important role of shelterbelts as geochemical barriers. They were shown to facilitate the lateral transport of substances from arable soils to the soils in the shelterbelts.

Along with lateral transport, there was a noticeable radial transport of substances in the forest soil profiles, especially the components of easily soluble salts from the deeper layers of soil-forming rocks to the lower part of the soil profiles (Figure 17). These findings can be used to enhance the theoretical foundations of environmental geochemistry, particularly in the concept of landscape–geochemical barriers [3,51].

Lastly, the fundamental application of this research is the justification of the shelterbelts and the adjacent spaces in agrolandscapes as independent natural–anthropogenic geosystems with their own structural organization and spatial connections of microstructural soil cover types (Figure 18). These results can contribute to the development of theoretical foundations in landscape studies and the theory of physico-geographical zoning of the Earth [52–54].

6. Conclusions

- From 1970 to 2020, there has been an increase in forested areas in the forest-steppe region of central eastern Europe. Within six model key sites covering an area of 1722 km² and located in different climatic conditions of the forest-steppe zone, the forest cover increased from 14% to 24% of the total area. The main processes contributing to the increase in forest cover were the planting of young protective shelterbelts on flat watersheds (in the 1970s–1980s) and the expansion of anti-erosional shelterbelts on slopes and gullies (throughout the entire period).
- The expansion of forested areas was driven by climate moisture increases in conjunction with rising temperatures during the growing season. In more humid conditions of the forest-steppe, afforestation occurred more intensively compared to the southeastern territories adjacent to the steppe zone. According to the calculations, afforestation should cease when the hydrothermal coefficient reaches 0.78, which corresponds to the southern part of the steppe zone.
- Based on mass measurements (n = 2086), the average linear growth of forest boundaries across the studied area during the specified period was 23.5 m. Forest expansion was faster on north-facing slopes compared to south-facing slopes (growth of 23.5 m and

22.6 m, respectively). The growth of forest vegetation on west-facing slopes was the highest among all the studied aspects and significantly exceeded that on east-facing slopes (growth of 25 m and 23.5 m, respectively). The main reason for the more active afforestation of west-facing slopes was the fact that they received more moisture from atmospheric precipitation carried by westward airflow.

- Alongside the observed increase in forest cover (primarily due to the expansion of anti-erosional shelterbelts), there was the observed simultaneous process of forest degradation in the study region, mainly due to the increased fragmentation and mortality of mature shelterbelts. A consistent increase in the degree of shelterbelt degradation was found when moving from northwest to southeast in the forest-steppe, i.e., towards a drier climate.
- We observed a tendency for the more intensive accumulation of soil moisture in the fields located to the west of the shelterbelts compared to those located to the east, as observed during a two-year monitoring period (2020, 2021, May–September) in two areas of the agroforestry landscape in the forest-steppe. This tendency was most pronounced in the 10 m zone of arable fields adjacent to the shelterbelts. This was because the arable fields on the windward (western) side of the shelterbelts received more moisture compared to the soils on the leeward (eastern) side.
- The spread of tree roots in different directions from the shelterbelts to the arable fields led to the lateral uptake of substances from the plowed soils into the soils of the shelterbelts. Tree roots under the shelterbelts also performed radial (vertical) uptake of substances from the deep soil layers. Thus, the role of shelterbelts as biogeochemical barriers becomes apparent, capable of forming local geochemical anomalies in soils.
- Striped microstructures in the soil cover, known as linear soil ecological zones, were formed under the shelterbelts and on adjacent arable plots. The formation of these stripes was influenced by various factors, including specific microclimatic conditions, different types of vegetation (forest and agricultural), variations in ecological conditions for soil fauna, and the impact of agricultural machinery that passes along the boundaries of the shelterbelts. Shelterbelts and their surrounding areas in agrolandscapes can be viewed as naturally evolving geosystems with a unique structural organization. They are an essential component of the contemporary geographical zoning of the territory.

Author Contributions: Y.G.C., M.A.S., A.N.G. and V.G.B. conceived and designed the methods and approaches as well as the field studies; A.R.L. and M.G.L. performed the climatic conditions and characteristics; E.A.T. and A.G.N. used GIS technologies and satellite data and created special maps. All authors have read and agreed to the published version of the manuscript.

Funding: This study was supported by the Russian Science Foundation, project no. 19-17-00056-II “Transformation of soils and soil cover under the influence of shelterbelts in agricultural lands within the South of the Central Russian Upland”.

Data Availability Statement: Data is contained within the article. Publicly available datasets were analyzed in this study. This data can be found here: <https://www.arcgis.com/home/webscene/viewer.html> (accessed on 7 September 2023).

Conflicts of Interest: The authors declare no conflict of interest.

References

1. Bonan, G.B. Forests and climate change: Forcings, feedbacks, and the climate benefits of forests. *Science* **2008**, *320*, 1444–1449. [[CrossRef](#)]
2. Bouwman, A.F.; Leemans, R. The role of forest soils in the global carbon cycle. In *Carbon Forms and Functions in Forest Soils*; McFee, W.W., Kelly, J.M., Eds.; Soil Science Society of America, Inc.: Madison, WI, USA, 1995; pp. 503–525.
3. Perelman, A.I.; Kasimov, N.S. *Landscape Geochemistry*; ASTREYA: Moscow, Russia, 1999; p. 768. (In Russian)
4. Hättenschwiler, S.; Tiunov, A.V.; Scheu, S. Biodiversity and litter decomposition in terrestrial ecosystems. *Annu. Rev. Ecol. Evol. Syst.* **2005**, *36*, 191–218. [[CrossRef](#)]
5. Lorenz, K. *Carbon Sequestration in Forest Ecosystems*; Springer: Dordrecht, The Netherlands, 2010; p. 279.

6. Osman, K.T. Physical Properties of Forest Soils. In *Forest Soils*; Springer: Dordrecht, The Netherlands, 2013; pp. 229–251.
7. FAO. Global Forest Resources. Available online: <https://www.fao.org/3/CA8753EN/CA8753EN.pdf> (accessed on 18 August 2023).
8. Alix-Garcia, J.; Munteanu, C.; Zhao, N.; Potapov, P.V.; Prishchepov, A.V.; Radeloff, V.C.; Krylov, A.; Bragina, E. Drivers of forest cover change in Eastern Europe and European Russia, 1985–2012. *Land Use Policy* **2016**, *59*, 284–297. [[CrossRef](#)]
9. *Voronezh Carved Wooden Boats*; The Affairs of the Don Region. Book Four; Russian Historical Library: St. Petersburg, Russia, 1913; Volume 29, pp. 154–155. (In Russian)
10. Ogloblin, N.N. *Overview of Historical and Geographical Materials of the 17th and Early 18th Centuries Contained in the Books of the Razryadny Prikaz*; Moscow, Russia, 1884; p. 369. (In Russian)
11. Duguma, L.A.; Minang, P.A.; van Noordwijk, M. Climate change mitigation and adaptation in the land use sector: From complementarity to synergy. *Environ. Manag.* **2014**, *54*, 420–432. [[CrossRef](#)] [[PubMed](#)]
12. Pérez-Silos, I.; Álvarez-Martínez, J.M.; Barquín, J. Large-scale afforestation for ecosystem service provisioning: Learning from the past to improve the future. *Landsc. Ecol.* **2021**, *36*, 3329–3343. [[CrossRef](#)]
13. Leah, T. Multifunctional role of protective forest plantations in the sustainable development of agricultural landscapes. In *Conservation of Plant Diversity*; Nauka: Moscow, Russia, 2017; p. 133.
14. Peskett, L.; MacDonald, A.; Heal, K.; McDonnell, J.; Chambers, J.; Uhlemann, S.; Upton, K.; Black, A. The impact of across-slope forest strips on hillslope subsurface hydrological dynamics. *J. Hydrol.* **2020**, *581*, 124427. [[CrossRef](#)]
15. Brandle, J.R.; Hodges, L.; Zhou, X.H. Windbreaks in North American agricultural systems. *Agroforest. Syst.* **2004**, *61*, 65–78.
16. Kort, J. Benefits of windbreaks to field and forage crops. In *Agriculture, Ecosystems & Environment*; Elsevier: Amsterdam, The Netherlands, 1988; Volume 22, pp. 165–190.
17. Perry, C.H.; Woodall, C.W.; Liknes, G.C.; Schoeneberger, M.M. Filling the gap: Improving estimates of working tree resources in agricultural landscapes. *Agroforest. Syst.* **2009**, *75*, 91–101. [[CrossRef](#)]
18. Erusalimsky, V.I.; Rozhkov, V.A. Multifunctional role of protective forest plantations. *Bull. Dokuchaev Soil Sci. Inst.* **2017**, *88*, 121–137. (In Russian) [[CrossRef](#)]
19. Chi, M.; Guo, Q.; Mi, L.; Wang, G.; Song, W. Spatial distribution of agricultural eco-efficiency and agriculture high-quality development in China. *Land* **2022**, *11*, 722. [[CrossRef](#)]
20. Xie, H.; Wang, G.G.; Yu, M. Ecosystem multifunctionality is highly related to the shelterbelt structure and plant species diversity in mixed shelterbelts of eastern China. *Glob. Ecol. Cons.* **2018**, *16*, e00470. [[CrossRef](#)]
21. Hernandez-Ramirez, G.; Sauer, T.J.; Cambardella, C.A.; Brandle, J.R.; James, D.E. Carbon sources and dynamics in afforested and cultivated Corn Belt soils. *Soil Sci. Soc. Am. J.* **2011**, *75*, 216–225. [[CrossRef](#)]
22. Kort, J.; Turnock, R. Carbon Reservoir and biomass in Canadian prairie shelterbelts. *Agroforest. Syst.* **1999**, *44*, 175–186. [[CrossRef](#)]
23. Schoeneberger, M.M. Agroforestry: Working trees for sequestering carbon on agricultural lands. *Agroforest. Syst.* **2009**, *75*, 27–37. [[CrossRef](#)]
24. Belevantsev, V.G.; Chendev, Y.G.; Terehin, E.A.; Lebedeva, M.G.; Solovyov, A.B. GIS-based analysis of forest cover change in Belgorod Oblast, Russia: 1780s–2010s. *Int. J. Geoinf.* **2019**, *15*, 11–18.
25. Rudolf, P.O.; Gevorkiantz, S.R. Shelterbelt experience in other lands. In *US Forest Service—Possibilities of Shelterbelt Planting in the Plains Region*; US Government Printing Office: Washington, DC, USA, 1935; pp. 59–76.
26. Milkov, F.N.; Nesterov, A.I.; Petrov, P.G.; Goncharov, M.V. *Kamennaya Steppe: Forest-Agrarian Landscapes*, 3rd ed.; Publishing House of Voronezh University: Voronezh, Russia, 1992; p. 224. (In Russian)
27. Turusov, V.I.; Lepikhin, A.A.; Chekanishkin, A.S. *Experience of FOREST Reclamation of Steppe Landscapes (on the 125th Anniversary of "Special Expedition... " by V.V. Dokuchaev)*; "Istoki" Publishing: Voronezh, Russia, 2017; p. 228. (In Russian)
28. Chendev, Y.G.; Sauer, T.J.; Ramirez, G.H.; Burras, C.L. History of East European Chernozem Soil Degradation; Protection and Restoration by Tree Windbreaks in the Russian Steppe. *Sustainability* **2015**, *7*, 705–724. [[CrossRef](#)]
29. Schroeder, W.R.; Kort, J. Shelterbelts in the Soviet Union. *J. Soil Water Cons.* **1989**, *44*, 130–134.
30. Potapov, P.V.; Turubanova, S.A.; Tyukavina, A.; Krylov, A.M.; McCarty, J.L.; Radeloff, V.C.; Hansen, M.C. Eastern Europe's forest cover dynamics from 1985 to 2012 quantified from the full Landsat archive. *Remote Sens. Environ.* **2015**, *159*, 28–43. [[CrossRef](#)]
31. Lu, J.; Huang, C.; Tao, X.; Gong, W.; Schleeweis, K. Annual forest disturbance intensity mapped using Landsat time series and field inventory data for the conterminous United States (1986–2015). *Remote Sens. Environ.* **2022**, *275*, 113003. [[CrossRef](#)]
32. Baumann, M.; Ozdogan, M.; Kuemmerle, T.; Wendland, K.J.; Esipova, E.; Radeloff, V.C. Using the Landsat record to detect forest-cover changes during and after the collapse of the Soviet Union in the temperate zone of European Russia. *Remote Sens. Environ.* **2012**, *124*, 174–184. [[CrossRef](#)]
33. Rendenieks, Z.; Nita, M.D.; Nikodemus, O.; Radeloff, V.C. Half a century of forest cover change along the Latvian-Russian border captured by object-based image analysis of Corona and Landsat TM/OLI data. *Remote Sens. Environ.* **2020**, *249*, 112010. [[CrossRef](#)]
34. Liu, F.; Liu, H.; Xu, C.; Zhu, X.; He, W.; Qi, Y. Remotely sensed birch forest resilience against climate change in the northern China forest-steppe ecotone. *Ecol. Indic.* **2021**, *125*, 107526. [[CrossRef](#)]
35. Shi, F.; Liu, M.; Qiu, J.; Zhang, Y.; Su, H.; Mao, X.; Li, X.; Fan, J.; Chen, J.; Lv, Y.; et al. Assessing land cover and ecological quality changes in the Forest-Steppe Ecotone of the Greater Khingan Mountains, Northeast China, from Landsat and MODIS observations from 2000 to 2018. *Remote Sens.* **2022**, *14*, 725. [[CrossRef](#)]

36. FAO; IUSS Working Group WRB. *World Reference Base for Soil Resources 2014, Update 2015; International Soil Resources Reports No. 106*; FAO: Rome, Italy, 2015. Available online: <https://www.fao.org/publications/card/en/c/942e424c-85a9-411d-a739-22d5f8b6cc41/> (accessed on 18 August 2023).
37. Selyaninov, G.T. On agricultural climate valuation. *Proc. Agric. Meteor.* **1928**, *20*, 165–177. (In Russian)
38. Kononova, M.M.; Belchikova, N.P. Quick methods of determining the humus composition of mineral soils. *Sov. Soil Sci.* **1961**, *12*, 1112–1121. (In Russian)
39. Visbeck, M.; Chassignet, E.P.; Curry, R.G.; Delworth, T.L.; Dickson, R.R.; Krahnmann, G. The ocean's response to North Atlantic Oscillation variability // The North Atlantic Oscillation: Climatic significance and environmental impact. *Geophys. Monogr.* **2003**, *134*, 113–146. [CrossRef]
40. Chendev, Y.G.; Hubbart, J.A.; Terekhin, E.A.; Lupo, A.R.; Sauer, T.J.; Burras, L.C. Recent afforestation in the Iowa River and Vorskla River Basins: A comparative trends analysis. *Forests* **2016**, *7*, 278. [CrossRef]
41. Alexandrovski, A.L.; Chendev, Y.G.; Yurtaev, A.A. Soils with the Second Humus Horizon, Paleochernozems, and the History of Pedogenesis at the Border between Forest and Steppe. *Eurasian Soil Sci.* **2022**, *55*, 125–144. [CrossRef]
42. Chendev, Y.; Aleksandrovskiy, A.; Khokhlova, O.; Skripkin, V. 14C Dating to study the development of soils in the Forest-Steppe of the Central Russian Upland as a result of bioclimatic changes and long-term cultivation. *Radiocarbon* **2018**, *60*, 1185–1198. [CrossRef]
43. Lukanina, E.; Shumilovskikh, L.; Novenko, E. Vegetation and fire history of the East-European forest-steppe over the last 14,800 years: A case study from Zamostye, Kursk region, Russia. *Palaeogeogr. Palaeoclimatol. Palaeoecol.* **2022**, *605*, 111218. [CrossRef]
44. Eckmeier, E.; Gerlach, R.; Gehrt, E.; Schmidt, M.W.I. Pedogenesis of Chernozems in central Europe—A review. *Geoderma* **2007**, *139*, 288–299. [CrossRef]
45. Kabała, C.; Przybył, A.; Krupski, M.; Łabaz, B.; Waroszewski, J. Origin, age and transformation of Chernozems in northern Central Europe—New data from Neolithic earthen barrows in SW Poland. *Catena* **2019**, *180*, 83–102. [CrossRef]
46. Vyslouzilova, B.; Ertlen, D.; Sefrna, L.; Novak, T.; Viragh, K.; Rue, M.; Campaner, A.; Dreslerová, D.; Schwartz, D. Investigation of vegetation history of buried Chernozem soils using near-infrared spectroscopy (NIRS). *Quart. Int.* **2015**, *365*, 203–211. [CrossRef]
47. Alexandrovsky, A.L.; Alexandrovskaya, E.I. *Evolution of Soils and Geographical Environment*, 3rd ed.; Nauka: Moscow, Russia, 2005; p. 223. (In Russian)
48. Klimanov, V.A.; Serebryannaya, T.A. Changes in vegetation and climate in the Central Russian Upland in the Holocene. *Izv. AN SSSR Ser. Geogr.* **1986**, *1*, 26–37. (In Russian)
49. Serebryannaya, T.A. Dynamics of the boundaries of the Central Forest-Steppe in the Holocene. In *Centuries of Biogeocenosis Dynamics; Readings in Memory of Academician V.N. Sukachev*; Nauka: Moscow, Russia, 1992; pp. 54–71. (In Russian)
50. Chendev, Y.G.; Tishkov, A.A.; Savin, I.Y.; Lebedeva, M.G.; Solovyev, A.B. Response of the soil and other components of the natural environment to climate change of different periodicity on the southern part of the Central Russian Upland. *Izv. RAN Geograph. Ser.* **2020**, *84*, 427–440. (In Russian)
51. Glazovskaya, M.A. Geochemical barriers in soils: Their typology, functional features, and ecological significance. In *Geochemistry of Landscapes and Soil Geography. 100 Years Since the Birth of M.A. Glazovskaya*; Kasimov, N.S., Gerasimova, M.I., Eds.; APR Moscow: Moscow, Russia, 2012; pp. 26–44. (In Russian)
52. Solntsev, N.A. *Landscape Studies: Selected Works*, 3rd ed.; MGU Publishing: Moscow, Russia, 2001; p. 383. (In Russian)
53. Isachenko, A.G. *Theory and Methodology of Geography*; Academia: Moscow, Russia, 2004; p. 400. (In Russian)
54. Milkov, F.N. *Physical Geography: Landscape Studies and Geographical Zonation*; Voronezh State University Publishing: Voronezh, Russia, 1986; p. 224. (In Russian)

Disclaimer/Publisher's Note: The statements, opinions and data contained in all publications are solely those of the individual author(s) and contributor(s) and not of MDPI and/or the editor(s). MDPI and/or the editor(s) disclaim responsibility for any injury to people or property resulting from any ideas, methods, instructions or products referred to in the content.